DEVELOPMENT OF A PICOSECOND PULSED MODE-LOCKED FIBER LASER

A THESIS SUBMITTED TO
THE GRADUATE SCHOOL OF NATURAL AND APPLIED SCIENCES
OF
MIDDLE EAST TECHNICAL UNIVERSITY

BY

MAHMUT EMRE YAĞCI

IN PARTIAL FULFILLMENT OF THE REQUIREMENTS
FOR
THE DEGREE OF MASTER OF SCIENCE
IN
PHYSICS

JANUARY 2013

Approval of the thesis:

DEVELOPMENT OF A PICOSECOND PULSED MODE-LOCKED FIBER LASER

Submitted by **MAHMUT EMRE YAĞCI** in partial fulfillment of the requirements for the degree of Master of Science in **Physics Department, Middle East Technical University** by,

Prof. Dr. Canan Özgen _____
Dean, Graduate School of **Natural and Applied Sciences**

Prof. Dr. Mehmet Zeyrek _____
Head of Department, **Physics**

Assoc. Prof. Dr. Hakan Altan _____
Supervisor, **Physics Dept., METU**

Dr. Halil Berberoğlu _____
Co-Supervisor, **Physics Dept., METU**

Examining Committee Members

Assoc. Prof. Dr. F. Ömer İlday _____
Physics Dept, Bilkent Univ.

Assoc. Prof. Dr. Hakan Altan _____
Physics Dept., METU

Dr. Halil Berberoğlu _____
Physics Dept., METU

Assist. Prof. Dr. Alpan Bek _____
Physics Dept., METU

Koray Eken, MSc _____
FiberLAST

Date: 30 January 2013

I hereby declare that all information in this document has been obtained and presented in accordance with academic rules and ethical conduct. I also declare that, as required by these rules and conduct, I have fully cited and referenced all material and results that are not original to this work.

Name, Last name: Mahmut Emre Yağcı

Signature :

ABSTRACT

DEVELOPMENT OF A PICOSECOND PULSED MODE-LOCKED FIBER LASER

Yağcı, Mahmut Emre
M.Sc., Department of Physics
Supervisor: Assoc. Prof. Dr. Hakan Altan

January 2013, 55 Pages

Fiber lasers represent the state-of-the-art in laser technology and hold great promise for a wide range of applications because they have a minimum of exposed optical interfaces, very high efficiency, and are capable of exceptional beam quality. In the near future, the most important markets such as micromachining, automotive, biomedical and military applications will begin to use this technology. The scope of this thesis is to design and develop a short picosecond pulsed fiber laser using rare-earth doped fiber as a gain medium. The proposed master oscillator power amplifier (MOPA) will be used to generate pulses with high repetition rates.

In this study, first we explain the basic theoretical background of nonlinear optics and fiber laser. Then, the numerical simulation will be introduced to explain how the laser system design and optimization. The simulation is based on nonlinear Schrödinger equation with the method of split-step evaluation. The brief theoretical background and simulation results of the laser system will be shown.

Finally, the experimental study of the developmental fiber laser system that comprises an oscillator, preamplifier and power amplifier will be discussed.

Keywords: Fiber laser, ytterbium doped fiber laser system, pulsed laser operation, high power laser.

ÖZ

PİKOSANİYE ATIMLI KİP-KİLİTLİ FİBER LAZER GELİŞTİRİLMESİ

Yağcı, Mahmut Emre
Yüksek Lisans., Fizik Bölümü
Tez Yöneticisi: Doç. Dr. Hakan Altan

Ocak 2013, 55 Sayfa

Fiber lazerler, günümüz lazer teknolojisinin ulaştığı en son gelişmedir. Bu teknolojinin çok geniş uygulama alanları olacağı umut edilmektedir bunun sebebi hassas optik parça gereksiniminin az olması, yüksek verimlilik, yüksek ışın kalitesi gibi özelliklerin bu teknolojiyi ön plana çıkarmasıdır. Yakın gelecekte hassas işleme, otomotiv, biomedical ve askeri uygulamalar gibi en önemli pazarlar bu teknolojiyi kullanmaya başlayacaklardır. Bu tez çalışması kapsamında, nadir toprak elementi katkılı kazanç fiberi kullanılarak pikosaniye atımlı fiber lazer geliştirilecektir. Yüksek frekansda yüksek enerjili atımlar elde etmek için ana osilatörlü güç yükselteci yöntemi kullanılacaktır.

Bu çalışmada öncelikle doğrusal olmayan optik ve fiber lazer ile ilgili teorik bilgiler verilmiştir. Daha sonra lazer sistemini dizayn ve optimize etmek için kullandığımız numerik simulasyon anlatılmıştır. Bu simulasyon doğrusal olmayan Schrödinger denklemini ayrık-adım tekniği ile çözme üzerine kuruludur. Simulasyon ile ilgili teorik bilgi ve simulasyondan elde edilen sonuçlar gösterilecektirmiştir.

Son olarak da geliştirilen sistem için yapılan deneysel çalışmaların sonuçları gösterilmiştir. Geliştirilen lazer sistemi, lazer salıngacı, önyükselteç ve güç yükseltecinden oluşmaktadır.

Anahtar Kelimeler: Fiber lazer, yttrebium katkılı fiber lazer sistemi, atımlı lazer operasyonu, yüksek güçlü lazerler.

To my dear Family

ACKNOWLEDGMENTS

I am most thankful to my supervisor Assoc. Prof. Dr. Hakan Altan and my co-supervisor Dr. Halil Berberoğlu for sharing their invaluable ideas and experiences on the subject of my thesis.

I am very grateful to FiberLAST throughout the production of my thesis.

I am indebted to Bülent Öktem, for their close collaboration when developing the laser system.

I would like to forward my appreciation to all my friends and colleagues especially Koray Eken, F. Ömer İlday and Yiğit Ozan Aydın, Mesut Tasalı who contributed to my thesis with their continuous encouragement.

I am grateful to Evren Togay, Nazmi Sedefoğlu, Turgut Aydemir, Bahtiyar Altemir, Fatih Yardım and Eren Yağcı for their support and friendship.

This work was supported by TÜBİTAK under grants 3110216.

TABLE OF CONTENTS

LIST OF TABLES

TABLES

LIST OF FIGURES

FIGURES

CHAPTER 1

INTRODUCTION

1.1 Brief History of Fiber Lasers

The development of the fiber technology was initiated with the development of the field of telecommunications. First, the telegraph by Samuel Morse in 1837, then the telephone by Alexander Graham Bell in 1878 started the rapid development in the communication area. In 1878, James C. Maxwell opened the way for discovering radio waves by Heinrich Hertz in 1888 and the first radio was developed by Guglielmo Marconi in 1895. For the first radios, the bandwidth was about 15 kHz and these days the maximum bandwidth of wireless communication is around a few hundred MHz. The reason of this limit is that free space propagation of signals is not suitable for reliable and fast communication links. As a solution, using a waveguide for light (or information) propagation was proposed but the development process took longer time. The basic phenomenon responsible for guiding of light in waveguides is total internal reflection. The first optical fibers were fabricated in 1920s [1-3]. However, these optical fibers did not have a cladding section thus these were not successful or effective in guiding light. After two major improvements, fiber optics showed remarkable advancement. First is the development of the cladded fibers in the 1950s [4-7], these types of fibers improved the guidance of light in the core of the fiber by surrounding it with also a silica cladding. The second improvement was the development of low loss fibers in 1979 [8]. The host material which is silica has nearly perfect purity for which Rayleigh scattering and material or infrared absorption at long wavelengths are at the fundamental limit for optical loss. Fig. 1.1 presents the loss characteristics of silica based fiber as a function of wavelength [9]. The minimum loss (about 0.2 dB/km) is at ~1.55 μm wavelength. This is the main reason as to why modern telecommunications use ~1. 55 μm wavelength.

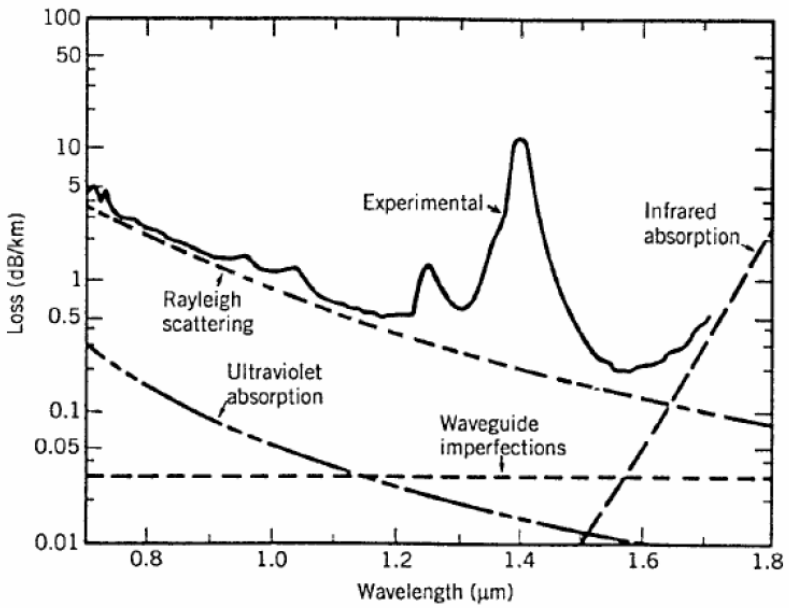

Figure 1.1 Loss characteristic of silica based fiber as a function of wavelength [9].

The developments in optical fibers led not only to advancements in telecommunications, but also to the birth of a new field, nonlinear fiber optics because the core of the fiber forced the intense light to travel in a small area for long distances. Hence, in the 1970s, "studies of nonlinear phenomena in optical fibers such as Raman and Brillouin scattering were conducted" [10-12], "followed by investigations in optically induced birefringence, parametric four-wave mixing and self-phase modulation" [13-17]. Soliton-like pulses supported by optical fibers as a result of interplay between the dispersion and nonlinearity were first suggested in 1973 [18] and observed experimentally in 1980 [19]. Availability of rare-earth doped (especially Erbium doped) fibers triggered the invention of the first fiber laser oscillators. Soliton-like mode-locked fiber lasers [20, 21] were followed by several other mode-locking regimes; stretched-pulse (dispersion-managed soliton) [22], similariton [23, 24], all-normal-dispersion (dissipative soliton) [25] and most recently soliton-similariton [26].

Fiber laser amplifiers mainly based on master-oscillator-power-amplifier design started to emerge after 1980s. The main factor holding back the high power amplifiers was the limited brightness of solid state diodes, which made it hard to couple more than ~1 W of pump power into the core of a fiber to amplify the signal. Solving this problem by using the double clad design [27] where the pump propagates through the cladding led to high power pump coupling into the fiber. Today fiber lasers can go up to 10 kW and their power level is reported to increase by a factor of ~1.7 each year [28]. Beam quality, robustness, and optical efficiency are important factors for fiber laser to become dominant over other types of lasers in several industry areas.

In this thesis we constructed a picosecond pulsed ytterbium doped fiber laser source and amplifier. The fiber laser system is a part of the project whose title is "Developing fiber laser system for industrial applications of precision micromachining". Although the purpose of development is precision micromachining, this application is not discussed in this thesis. Thus, the only fiber laser system is discussed throughout the thesis.

After the introduction, the next chapter will explain the theoretical background of fiber laser which includes pulse propagation, mode locking theory, amplification process and main limitations for fiber lasers. The chapter three will summarize the numerical simulation for fiber laser that contains an explanation of the numerical method and obtained simulation results for fiber laser. The chapter four will explained all experimental works during the development of fiber laser source and amplifiers. The chapter five will summarize all studies.

CHAPTER 2

THEORETICAL BACKGROUND OF FIBER LASER

2.1 Optical Fibers

Although there are lots of other fiber designs, the simplest one is seen in Fig. 2.1, which is called as the step-index fiber and composed of a fused silica glass core with a refractive index of n_1 surrounded by also a glass cladding with a slightly lower index of n_2.

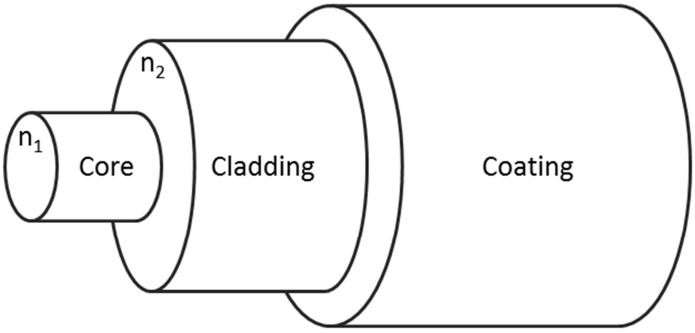

Figure 2.1 Step-index fiber diagram

Light is guided in the core by total internal reflection at the core/cladding interface. Two basic parameters of this structure are the index difference, which determines the numerical aperture (*NA*) of the fiber as

$$NA = (n_1^2 - n_2^2)^{1/2} \tag{2.1}$$

and the core radius , which determines the normalized frequency (*V*-parameter) of the fiber together with the numerical aperture and the wavenumber $k_0 = w/c = 2\pi/\lambda$ as

$$V = k_0 a NA \tag{2.2}$$

V-parameter is particularly important since it is related to the number of modes that an optical fiber can support. For single-mode operation, it should be less than 2.405. The cladding radius is not so important as long as the evanescent field of the light stays within the cladding.

2.2 Nonlinear Optics

Nonlinear optics defines as a modification of the optical properties of a material when interacting with light existence. The high intense light is needed to change the optical properties of a matter. After the realization of nonlinear optics, this phenomenon was considered as a problem for optical researches, however later turned into the basis of ultrafast laser technology.

The nonlinearity happens when the response of a material is “nonlinear” with respect to applied light. For instance, the occurrence of harmonic generation depends on the intensity of the applied field, i.e. the square of the applied field creates second harmonic generation, and cube of the applied field creates third harmonic generation as well as other processes.

Polarization is an important factor in defining nonlinear optics. It will be explained in detail in section 2.4. The nonlinear wave equation is [29],

$$\nabla^2 E - \frac{1}{c^2}\frac{\partial^2 E}{\partial t^2} = \mu_0 \frac{\partial^2 P^{NL}}{\partial t^2} \tag{2.3}$$

where *c* is the speed of light in vacuum and *n* is the linear refractive index.

In linear optics, polarization $P(t)$ of a substance is related to the field strength $E(t)$ as [29];

$$P(t) = \varepsilon_0 \chi^{(1)} E(t) \tag{2.4}$$

where $\chi^{(1)}$ is the linear susceptibility of the substance. However, the Equation (2.4) does not describe the nonlinear response of substances. The electromagnetic wave creates non-harmonic motion of bound electrons in the substance; consequently, polarization $P(t)$ is defined the more appropriate equation (2.5) [29];

$$P(t) = \varepsilon_0 \left(\chi^{(1)} E(t) + \chi^{(2)} E^2(t) + \chi^{(3)} E^3(t) \ldots\right) \tag{2.5}$$

$$\equiv P_{linear} + P_{nonlinear} \tag{2.6}$$

where $\chi^{(2)}$ and $\chi^{(3)}$ represent the second and third-order nonlinear optical susceptibilities. In equations (2.5) and (2.6), P_{linear}, the linear term is the leading factor for the total polarization of the substance. The remaining terms are the correction elements that are needed for compensation of intense electromagnetic field on polarization. As we can think, the propagation of electromagnetic wave in optical fiber is governed by Maxwell’s equations where the wave equation is derived. Nonlinear terms of the polarization can be also put into the electromagnetic wave equation which is converted to a nonlinear differential equation that has special solutions (the propagation of the light in optical fibers shall be explained in later subsections). $P^{(2)}(t)$, the second term of nonlinear polarization creates nonlinear process such as *Second-Harmonic Generation,* while $P^{(3)}(t)$, the third term of nonlinear polarization creates nonlinear effect such as *Kerr Nonlinearity*, both of them shall be examined in detail in following subsections. $P^{(2)}(t)$ happens in material with molecular level lacking inversion symmetry (centrosymmetric media), as it is known that

the second term of nonlinear polarization is zero for gases, liquids, most crystals, and amorphous solids(i.e. glass) due to inversion symmetry. Nevertheless, the third term of nonlinear polarization can happen both in symmetric and non-symmetric molecular structures. This difference explains the fact that despite the high optical power, it is not observed generation of second harmonic in a fiber and free-space laser cavity. Besides, it also explains why birefringent crystals produce second harmonic generation inside a laser cavity. Likewise, it is also the reason why the leading nonlinear effect in a fiber laser is the weaker third order polarization term.

A simple approximation of susceptibility values can be calculated in this way. "The second order polarization term $P^{(2)}(t)$ would be significant enough regarding linear term $P^{(1)}(t)$ when the amplitude of the applied field strength E is on the order of atomic electric field strength $E_{at}=e/a_o^2$ where e is the electron charge and $a_o=\hbar/me^2$ is the Bohr radius of the hydrogen atom ($\hbar$ is Planck's constant divided by 2π and m is the electron mass). Substituting the values of physical constants $\hbar$, m and e from literature, E_{at} is found to be $6.\widehat{66} \times 10^6$ m/V. Thus the second-order susceptibility $\chi^{(2)}$ would be on the order of $\chi^{(1)}/E_{at}$. $\chi^{(1)}$ is almost unity of condensed matter, so $\chi^{(2)}$ value for condensed matter is given as" [29];

$$\chi^{(2)} \approx 2.09 \times 10^{-11} \text{ m/V} \tag{2.7}$$

"Likewise, $\chi^{(3)}$ would be on the order of $\chi^{(1)}/E_{at}^2$, which has a value for condensed matter" [29];

$$\chi^{(3)} \approx 4.2 \times 10^{-23} \text{ m}^2/\text{V}^2 \tag{2.8}$$

These approximated non-linear susceptibility values give us a prediction why we need high intensity levels to observe the nonlinear effects in optical media.

In this section, some of parametric and non-parametric nonlinear optical processes will be examined shortly. It will be also clarified how they can be joined into Equation (2.5), the total polarization relation. Nevertheless, these nonlinear optical processes are beyond the scope of this thesis, therefore only the nonlinear processes which include the physics in fiber lasers will be explained comprehensively in following subsections.

Second Harmonic Generation (SHG):

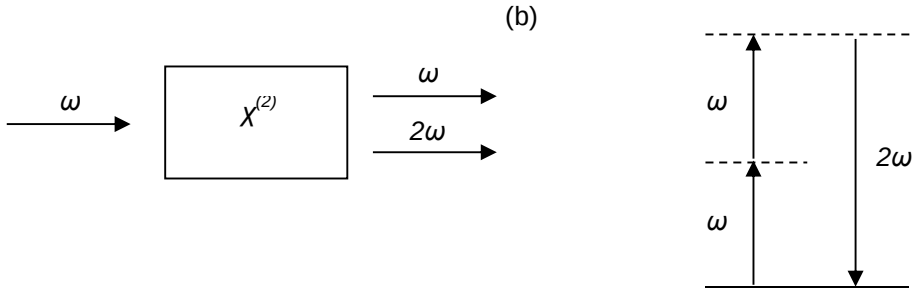

Figure 2.2 (a) Diagram of SHG. (b) Energy-level diagram SHG.

“In second-harmonic generation two photons at the same frequency ω are vanished and a photon of frequency of 2*ω* is created in a single quantum mechanical process. This is illustrated in Figure 2.2.a. In Figure 2.2.b, the solid line is the ground state and the dashed lines are the virtual levels, which represent essentially the combined energy of one of the energy eigenstates of the atom and of one or more photons of the radiation field” [29]

“In theory a laser beam with electric field” [29];

$$E(t) = Ee^{-i\omega t} + c.c. \tag{2.9}$$

is incident upon an optical medium with a nonzero second order susceptibility $\chi^{(2)}$ then the second order polarization term which is produced in such an optical medium is defined by [29];

$$P^{(2)}(t) = \varepsilon_0\chi^{(2)}E^2(t) = 2\varepsilon_0\chi^{(2)}EE^* + \left(\varepsilon_0\chi^{(2)}E^2e^{-2\omega t} + c.c.\right) \tag{2.10}$$

“In Equation 2.10, the nonlinear polarization comprises a contribution at zero frequency and a contribution of frequency 2*ω.* According to Equation (2.3), the nonlinear electromagnetic wave relation, contribution at frequency 2*ω* causes the generation of radiation in the second-harmonic frequency. However, contribution at zero frequency cannot cause the generation of any electromagnetic radiation because its second time derivative is zero.”

Sum Frequency Generation (SFG):

(a) (b)

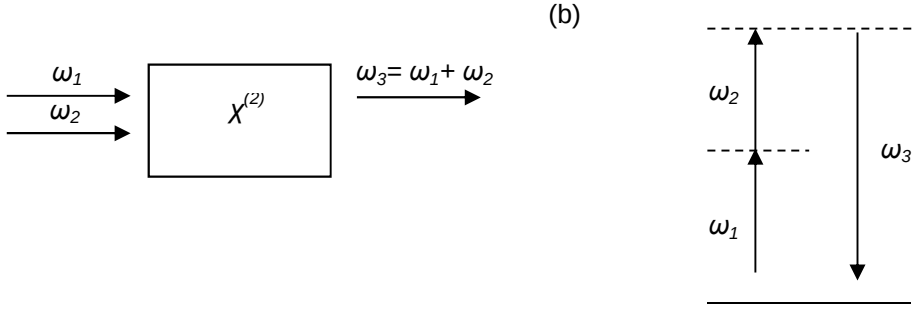

Figure 2.3 (a) Diagram of SFG. (b) Energy-level diagram SFG

Sum-frequency generation is similar second-harmonic process, excepting in sum-frequency generation the two incoming photon frequencies are different which is shown in Figure 2.3.a. If the certain photons with electric field *E(t)* (2.9) is incident upon an optical medium with nonzero second order susceptibility $\chi^{(2)}$, the second order polarization term which is produced in sum-frequency generation is defined by [29];

$$P(\omega_1 + \omega_2) = 2\varepsilon_0\chi^{(2)}E_1E_2 \tag{2.11}$$

Difference Frequency Generation (DFG):

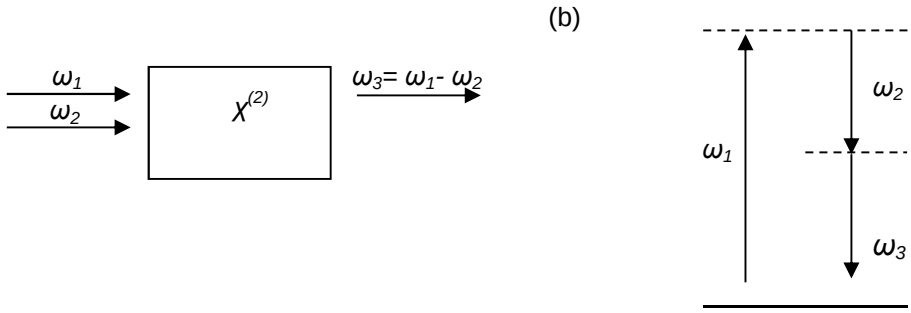

Figure 2.4 (a) Diagram of DFG. (b) Energy-level diagram DFG

In difference-frequency generation, two photons with different frequencies are inputs for the optical medium then the photon whose frequency is difference of incoming photons is created (Figure 2.4). The generation is explained by the second order polarization term [29];

$$P(\omega_1 - \omega_2) = 2\varepsilon_0 \chi^{(2)} E_1 E_2^* \tag{2.12}$$

To think about the overall process of a second order harmonic generation, suppose a medium with electric field [29];

$$E(t) = Ee^{-i\omega_1 t} + Ee^{-i\omega_2 t} + c.c. \tag{2.13}$$

is incident upon a optical medium with nonzero second order susceptibility $\chi^{(2)}$. then the second order polarization term which is produced in such an optical medium is defined by [29];

$$P^{(2)}(t) = \varepsilon_0 \chi^{(2)} [E_1^2 e^{-2i\omega_1 t} + E_2^2 e^{-2i\omega_2 t} + 2E_1 E_2 e^{-i(\omega_1+\omega_2)t}$$

$$+2E_1 E_2^* e^{-i(\omega_1-\omega_2)t} + c.c] + 2\varepsilon_0 \chi^{(2)} [E_1 E_1^* + E_2 E_2^*] \tag{2.14}$$

Each of the complex components of the different frequency elements of this second order polarization term is related to different nonlinear process. First two components represent the SHG process, third component is the SFG process and the last component is corresponding to DFG process. Nevertheless, we should pay attention that at same instant only one of these frequency elements will be supported in an optical medium. This is because these parametric nonlinear generations require particular phase-matching condition.

Third Order Polarization:

When the $\chi^{(3)}$ term is nonzero, the third-order polarization component in a nonlinear medium is described by [29];

$$P^{(3)}(t) = \varepsilon_0 \chi^{(3)} E^3(t) \tag{2.15}$$

To generalize the process, one can suppose that the electric field comprising three frequency elements interact with the nonlinear medium [29];

$$E(t) = Ee^{-i\omega_1 t} + Ee^{-i\omega_2 t} + Ee^{-i\omega_3 t} + c.c. \tag{2.16}$$

Nevertheless, inserting $E^3(t)$ to the third order polarization term is quite complicated. The calculated $E^3(t)$ includes 44 frequency terms. For this reason, the convenient and sufficient electric field that has only one frequency term is described as [29];

$$E(t) = \mathcal{E} cos\omega t \tag{2.17}$$

Using well-known trigonometric relation, $cos^3\omega t = \frac{1}{4}cos3\omega t + \frac{3}{4}cos\omega t$, the third order polarization might be considered as [29];

$$P^{(3)}(t) = \frac{1}{4}\varepsilon_0 \chi^{(3)} \mathcal{E}^3 cos3\omega t + \frac{3}{4}\varepsilon_0 \chi^{(3)} \mathcal{E}^3 cos\omega t \tag{2.18}$$

The terms of equation (2.18) states different nonlinear process that shall be shortly explained below.

Third Harmonic Generation (THG):

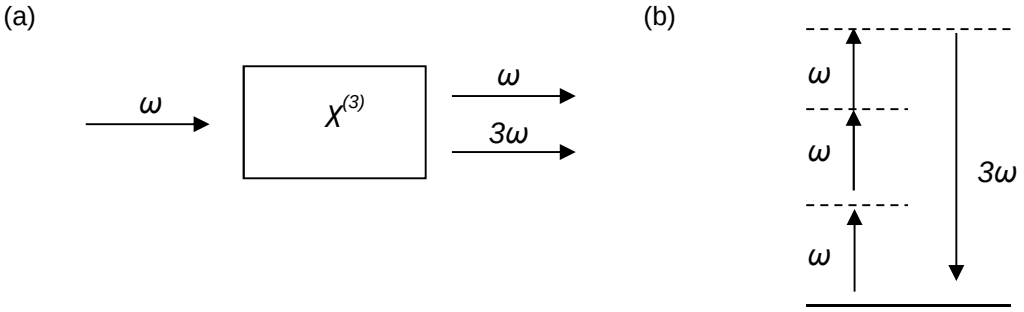

Figure 2.5 (a) Diagram of THG. (b) Energy-level diagram THG

The incident electric field at frequency ω produces new frequency component at 3ω with THG nonlinear effect. The first term of the Equation (2.18) represent for this new frequency component. This term explains third-harmonic generation that is shown in Figure 2.5. For THG process, the photon at frequency 3ω is created by three photons at frequency .

Intensity Dependent Refractive Index:

The second term of equation 2.18 is related to nonlinear refractive index with the incident optical field at frequency ω. The nonlinear refractive index might be given [29];

$$n = n_0 + n_2 I \tag{2.19}$$

"where n_0 is the linear refractive index and n_2 is an optical constant that decides the strength of the optical nonlinearity and *I* is the intensity of the incident field" [29].

The nonlinear effect is commonly called as *Kerr nonlinearity* that has great importance in fiber lasers.

The all nonlinear effects that are introduced above are known as parametric processes. In parametric nonlinear effects, the quantum mechanical states of the system do not change after interacting with nonlinear medium. On the contrary, in nonparametric processes, the first and last quantum mechanical states of the system have different real levels. There are basically two differences in parametric and nonparametric processes. The parametric process is defined by a real susceptibility, while the nonparametric process might be defined by a complex susceptibility. Besides, the second difference is that the energy the photon must be conserved in a parametric process; on the contrary, the energy of the photon does not have to be conserved in a nonparametric process. The subsequent two subtitles are examples of nonparametric processes.

Saturable Absorption:

Absorption coefficient of many substances reduces when high intense laser beam is incident upon the substance. The phenomenon is known as saturable absorber. The equation (2.22) is described process where α is measured absorption coefficient and the *I* intensity of the incident field [29];

$$\alpha = \frac{\alpha_0}{1 + I/I_s} \tag{2.22}$$

"where α_0 is the low-intensity absorption coefficient and I_s is the saturation intensity" [29].

Saturable absorption has an important factor in the concept of mode-locking of lasers therefore the effect of saturable absorber in laser oscillators shall be explained in detail in Section 2.6.

Two-Photon Absorption:

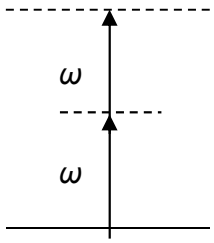

Figure 2.6 Energy-level diagram of two-photon absorption.

The two-photon absorption phenomenon (shown in Figure 2.6) is defined that a material absorbs simultaneously two photons from its ground state to an excited state. Conversely to linear optics, in the two-photon absorption process the absorption coefficient increases linearly with laser intensity. The relation can be given as [29];

$$\sigma = \sigma^{(2)} I \tag{2.23}$$

The coefficient $\sigma^{(2)}$ represents the two-photon absorption. Furthermore, the rate of atomic transition R because of two-photon absorption is related to the square of the optical field intensity, as it is known that $R = \sigma I/\hbar\omega$, hence [29];

$$R = \frac{\sigma^{(2)} I^2}{\hbar\omega} \tag{2.24}$$

Stimulated Raman Scattering:

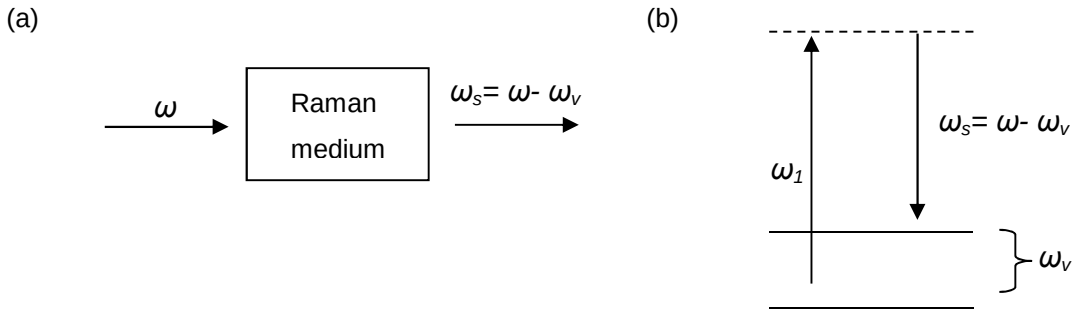

Figure 2.7 Illustration and energy-level diagram of stimulated Raman scattering

“Stimulated Raman scattering (SRS) shown in Fig. 2.7 and stimulated Brillouin scattering (SBS) are similar to each other. In these processes, the incident photon at frequency is annihilated and a photon at the Stokes frequency is created, leaving the atom (molecule) in an (vibrational) excited state with energy after the scattering, which corresponds to either an optical (SRS) or an acoustic phonon (SBS). Due to the very limited gain bandwidth of the SBS process, it is not effective and can be safely ignored for the broadband optical spectra as required for ultrashort pulse propagation. However, SRS can be a significant contributor for ultrashort pulses and must, in general, be taken into account.” [29].

2.3 Dispersion

Dispersion can be defined as the propagation of different frequency components with different velocities. Mainly there are three types of dispersion; material, waveguide and modal dispersions. The most dominant one is the material dispersion (or chromatic dispersion), which arises from the dependency of refractive index $n(\omega)$ on frequency. This is related to the characteristic resonant absorption frequencies of the medium. The Sellmeier equation gives a very successful approximation of the refractive index for frequencies far from these resonances [30];

$$n^2 = 1 + \sum_{j=1}^{m} \frac{B_j \omega_j^2}{\omega_j^2 - \omega^2} \tag{2.25}$$

where ω_j is the resonance frequency and B_j is its strength. The resonant wavelengths of silica are given as 0.0684 μm, 0.116 μm, 9.896 μm with strengths of 0.696, 0.408, 0.897, respectively [30]. Naturally, there are no resonances in the wavelength range where the silica fibers are commonly used (0.3−2.0 μm).

Waveguide dispersion occurs since the different frequency components in a waveguide have different propagation constants along the propagation direction. Modal dispersion is also similar; different modes in a waveguide have different propagation constants. In general the effect of modal dispersion is larger than the waveguide dispersion. However, it does not exist for a single-mode fiber.

Although dispersion is important in fiber optics in general, it is particularly important for the short pulse propagation, as it is very effective in broadening the pulse. After defining the dispersion which is related to the propagation constant $\beta(\omega)$, we can now write its Taylor expansion about where the pulse spectrum is centered [30]:

$$\beta(\omega) = n(\omega)\frac{\omega}{c} = \beta_0 + \beta_1(\omega - \omega_0) + \frac{1}{2!}\beta_2(\omega - \omega_0)^2 + \cdots \quad .(2.26)$$

Where $n(\omega) = n_{eff}(\omega)$ is the effective index of the fiber and $\beta_n = d^n\beta/d\omega^n$ is evaluated at $= \omega_0$. We can write few terms of this expansion, which are of physical significance [30]:

$$\beta_0 = \frac{1}{c} n(\omega_0)\omega_0 \quad .(2.27)$$

$$\beta_1 = \frac{1}{c}\left(n(\omega) + \omega\frac{dn(\omega)}{d\omega}\right)_{\omega_0} = \frac{n_g}{c} = \frac{1}{v_g} \quad .(2.28)$$

$$\beta_2 = \frac{1}{c}\left(2\frac{dn(\omega)}{d\omega} + \omega\frac{d^2n(\omega)}{d\omega^2}\right)_{\omega_0} \quad .(2.29)$$

Where n_g is the group index and v_g is the group velocity. Physically, the envelope of a pulse propagates with the group velocity β_1^{-1} while β_2 represents the dispersion of group velocity responsible for broadening of the pulse. So β_2 is known as the group velocity dispersion (GVD) parameter. Sometimes the dispersion parameter *D* is used in place of β_2, which are related to each other by the following equation [30]

$$D = \frac{d\beta_1}{d\lambda} = -\frac{2\pi c}{\lambda^2}\beta_2 \cong \frac{\lambda}{c}\frac{d^2n(\lambda)}{d\lambda^2} \quad (2.30)$$

Where $\lambda = 2\pi c/\omega$ is the wavelength corresponding to the frequency ω.

2.4 Pulse Propagation in Fiber Laser

The process of the pulse propagation in optical fibers is governed by Maxwell's equations like all other electromagnetic phenomena;

$$\nabla.\boldsymbol{D} = \rho \quad (2.31)$$

$$\nabla.\boldsymbol{B} = 0 \quad (2.32)$$

$$\nabla \times \boldsymbol{E} = -\frac{\partial \boldsymbol{B}}{\partial t} \quad (2.33)$$

$$\nabla \times \boldsymbol{H} = \boldsymbol{j} + \frac{\partial \boldsymbol{D}}{\partial t} \quad (2.34)$$

In the equations, ***B*** and ***D*** represent magnetic and electric flux densities, respectively. Besides, ***H*** and ***E*** are related to magnetic and electric field vectors, respectively. Free charges ρ and current density ***j*** disappear, because there are no free charges in optical fibers. It is known that the magnetic and electric flux densities are related to electric and magnetic fields and this relation can be defined as;

$$\boldsymbol{D} = \varepsilon_0\boldsymbol{E} + \boldsymbol{P} \quad (2.35)$$

$$\boldsymbol{B} = \mu_0\boldsymbol{H} + \boldsymbol{M} \quad (2.36)$$

where ***P*** and ***M*** are induced electric and magnetic polarizations, ε_0 is the vacuum permittivity, μ_0 is the vacuum permeability respectively. It is known that ***M*** is zero for a nonmagnetic medium like optical fibers. The use of the mathematical relation $\nabla \times (\nabla \times \boldsymbol{A}) = \nabla(\nabla.\boldsymbol{A}) - \nabla^2\boldsymbol{A}$ and calculating the curl of Equation (2.33) gives;

$$\nabla(\nabla.\boldsymbol{E}) - \nabla^2\boldsymbol{E} = -\frac{\partial}{\partial t}(\nabla \times \boldsymbol{B}) \quad (2.37)$$

Then inserting Equations (2.34), (2.35) and (2.36) we can acquire;

$$\nabla \times \boldsymbol{B} = \mu_0\varepsilon_0\frac{\partial \boldsymbol{E}}{\partial t} + \mu_0\frac{\partial \boldsymbol{P}}{\partial t} \quad (2.38)$$

One can calculate the following equation by substituting Equation (2.38) in (2.37). The equation depends on ***E*** and ***P*** only;

$$\nabla(\nabla.\boldsymbol{E}) - \nabla^2\boldsymbol{E} = -\mu_0\varepsilon_0\frac{\partial^2\boldsymbol{E}}{\partial t^2} - \mu_0\frac{\partial^2\boldsymbol{P}}{\partial t^2} \tag{2.39}$$

In homogenous medium, $\nabla.\boldsymbol{E}$ is zero due to no free charge in the medium. Besides, use of the equality $\mu_0\varepsilon_0 = 1/c^2$, one can simplify the Equation (2.39) to the wave equation;

$$\nabla^2\boldsymbol{E} - \frac{1}{c^2}\frac{\partial^2\boldsymbol{E}}{\partial t^2} = \mu_0\frac{\partial^2\boldsymbol{P}}{\partial t^2} \tag{2.40}$$

While solving this equation for the fiber modes, we assumed that the nonlinear part of the polarization is small and ignorable. This is acceptable for calculating the fiber modes but for short pulse propagation we have to include the nonlinear part since the intensity at the peak of an ultrashort pulse can be extremely high. When only the linear polarization is considered, it is straightforward to take the Fourier transform of the wave equation and write it in frequency domain. However, if the nonlinear part is included, this is not an easy task. Before starting to solve the equation, we have to assume that the polarization response of the medium is instantaneous. This is a good assumption for the electronic response because the reconfiguration time of an electron cloud is <1fs. However, the vibrational response can be quite slow (~60 fs for Raman scattering) and will be included later in this section.

In general, polarization can be written in terms of the powers of instantaneous electric field;

$$\boldsymbol{P}(\boldsymbol{r},t) = \underbrace{\varepsilon_0\big(\chi^{(1)}\boldsymbol{E}(\boldsymbol{r},t)}_{\boldsymbol{P}_L} + \underbrace{\chi^{(2)}\boldsymbol{E}^2(\boldsymbol{r},t) + \chi^{(3)}\boldsymbol{E}^3(\boldsymbol{r},t)\ldots\big)}_{\boldsymbol{P}_{NL}} = \boldsymbol{P}_L + \boldsymbol{P}_{NL} \tag{2.41}$$

"The electric field has a time structure that has a rapidly and slowly varying component. The slow timescale is the width of the pulse, which is typically on the order of 100 fs. The fast timescale is the optical cycle, which is on the order of $\lambda/c \approx 3$ fs. Hence it is useful to separate the timescales of electric field and polarization components in the form" [29];

$$\boldsymbol{E}(\boldsymbol{r},t) = \frac{1}{2}\boldsymbol{x}[E(\boldsymbol{r},t)\exp(i\beta_0 z - i\omega_0 t) + c.c.] \tag{2.42}$$

$$= \frac{1}{2}\boldsymbol{x}[F(x,y)A(z,t)\exp(i\beta_0 z - i\omega_0 t) + c.c.] \tag{2.43}$$

$$\boldsymbol{P}_L(\boldsymbol{r},t) = \frac{1}{2}\boldsymbol{x}[P_L(\boldsymbol{r},t)\exp(i\beta_0 z - i\omega_0 t) + c.c.] \tag{2.44}$$

$$\boldsymbol{P}_{NL}(\boldsymbol{r},t) = \frac{1}{2}\boldsymbol{x}[P_{NL}(\boldsymbol{r},t)\exp(i\beta_0 z - i\omega_0 t) + c.c.] \tag{2.45}$$

"Only the real part of the above equations is physically relevant, hence complex conjugate parts will not be stated anymore. Here, $\boldsymbol{x}$ is the unit vector perpendicular to the

propagation direction, which can be ignored because of the assumption that the polarization is maintained during the propagation through the fiber. $E(\boldsymbol{r},t)$ and $P_{L/NL}(\boldsymbol{r},t)$ are the slowly varying envelopes of the corresponding components. For future simplifications, the dependencies on x and y (modal pattern) from that on z and t (propagation) are separated. This is appropriate because the transverse mode structure in the fiber is to first order independent of propagation length and time. The quickly varying parts in both z and t are expressed as a plane wave that propagates in the z-direction and in a medium with effective index n" [29].

From the Equation (2.41), nonlinear polarization can be defined by using the fact $\chi^{(2)} = 0$ for optical fibers [30, 31]

$$\boldsymbol{P}_{NL}(\boldsymbol{r},t) = \varepsilon_0 \varepsilon_{NL}(\boldsymbol{r},t) E(\boldsymbol{r},t) \tag{2.46}$$

where the dielectric coefficient is assumed to be locally constant with a value of [30];

$$\varepsilon_{NL}(\boldsymbol{r},t) = \frac{3}{4}\chi^{(3)}|E(\boldsymbol{r},t)|^2 \tag{2.47}$$

When using the slowly varying amplitude $E(\boldsymbol{r},t)$ assumption to get the wave equation, it is convenient to work in the Fourier space. Nevertheless, we know that ε_{NL} has intensity dependence hence we cannot apply a Fourier transform. For this reason, we have to make perturbative assumption of $\boldsymbol{P}_{NL}$. The assumption is that the dielectric coefficient is assumed to be locally constant value. Substituting Equations (2.42) through (2.45) in Equation (2.40), the Fourier transform $\tilde{\mathrm{E}}(r,\omega-\omega_0)$, defined as [30];

$$\tilde{\mathrm{E}}(\boldsymbol{r},\omega-\omega_0) = \int_{-\infty}^{\infty} E(\boldsymbol{r},t)\exp[i(\omega-\omega_0)t]dt \tag{2.48}$$

is found to satisfy the Helmholtz equation [30];

$$\left(\nabla^2 + \varepsilon_{NL}(\boldsymbol{r},\omega)\frac{\omega^2}{c^2}\right)\tilde{\mathrm{E}}(\boldsymbol{r},\omega) = 0 \tag{2.49}$$

where the dielectric relation defined by [30]

$$\varepsilon(\omega) = 1 + \varepsilon_L + \varepsilon_{NL} \tag{2.50}$$

By means of separation of variables method, one can solve the Equation (2.49). The form of the solution is as [30];

$$\tilde{\mathrm{E}}(\boldsymbol{r},\omega-\omega_0) = F(x,y)\tilde{A}(z,\omega-\omega_0)\exp(ik_0 z) \tag{2.51}$$

Equation (2.51) is the Fourier transform of Equation (2.43). it is supposed that $\tilde{A}(z,\omega)$ and $F(x,y)$ are two part of the slowly varying function. $\tilde{A}(z,\omega)$ defines the pulse propagation and $F(x,y)$ defines the modal pattern in the fiber. Additional calculations give two equations for $F(x,y)$ and $\tilde{A}(z,\omega)$ [30];

$$\frac{\partial^2 F}{\partial x^2}+\frac{\partial^2 F}{\partial y^2}+\left[\varepsilon(\omega)\frac{\omega^2}{c^2}-\tilde{\beta}^2(\omega)\right]F=0 \tag{2.52}$$

$$2i\beta_0\frac{\partial \tilde{A}}{\partial z}+\left(\tilde{\beta}^2(\omega)-\beta_0^2\right)\tilde{A}=0 \tag{2.53}$$

In the second equation, we can neglect the first term with the second derivative because $\tilde{A}(z,\omega)$ is supposed to be propagation part of the slowly varying function. The first equation must be solved in order to find the fiber mode distribution and propagation constant β_0. Inclusion of nonlinear polarization term has no effect on $F(x,y)$ but is slightly modified β_0 as follows, additional calculation might be found in [30, 31]. The dielectric function in Equation (2.52) can be approximated as [30];

$$\varepsilon(\omega)=(n(\omega)+\Delta n)^2\approx n^2+2n\Delta n \tag{2.54}$$

where Δn is the nonlinearity of the refractive index, the absorption $\tilde{\alpha}$ and gain $\tilde{g}$ in the fiber implicitly embedded into as [30];

$$\Delta n=n_2|E|^2+\frac{i\tilde{\alpha}(\omega)-\tilde{g}(\omega)}{2k_0} \tag{2.55}$$

The nonlinear refractive index leads a corresponding nonlinear term in the propagation constant, which can be expressed as [30];

$$\tilde{\beta}(\omega)=\beta(\omega)+\Delta\beta(\omega) \tag{2.56}$$

and calculated from

$$\Delta\beta(\omega)=\frac{\omega^2 n(\omega)}{c^2\beta(\omega)}\frac{\int\int_{-\infty}^{\infty}\Delta n(\omega)|F(x,y)|^2dxdy}{\int\int_{-\infty}^{\infty}|F(x,y)|^2dxdy} \tag{2.57}$$

Only single-mode fibers are taken into consideration here and we can think about the $F(x,y)$ corresponding to the modal distribution of the fundamental fiber mode HE_{11} shown as [30];

$$F(x,y)=J_0(p\rho),\quad \rho=\sqrt{x^2+y^2}\le a \tag{2.58}$$

inside the core and;

$$F(x,y)=\sqrt{a/\rho}J_0(p\rho)\exp[-q(\rho-a)],\ \ \rho\ge a \tag{2.59}$$

outside the core. We should note that the shape of the fundamental mode is very similar to a Gaussian so in practice it is generally approximated by a Gaussian function in the form of

$$F(x,y)=\exp[-(x^2+y^2)/w^2] \tag{2.60}$$

Inserting Equation (2.56) into Equation (2.53) and then rewriting Equation (2.53) by using the assumption that $\tilde{\beta}(\omega)$ and β_0 are very close to each other so we can use $\tilde{\beta}^2(\omega) - \beta_0^2 \cong 2\beta_0(\tilde{\beta}^2(\omega) - \beta_0)$ [30];

$$\frac{\partial \tilde{A}}{\partial z} = i[\beta(\omega) + \Delta\beta(\omega) - \beta_0]\tilde{A} \tag{2.61}$$

Now, if we write Taylor series expansion of $\beta(\omega)$ about ω_0 ;

$$\beta(\omega) = \beta_0 + (\omega - \omega_0)\beta_1 + \frac{1}{2}(\omega - \omega_0)^2\beta_2 + \frac{1}{6}(\omega - \omega_0)^3\beta_3 + \cdots \tag{2.62}$$

where $\beta_0 \equiv \beta(\omega_0)$ and,

$$\beta_n = \left.\frac{d^n\beta}{d\omega^n}\right|_{\omega=\omega_0} \quad (m = 1,2, \dots) \tag{2.63}$$

“The cubic and higher-order terms in the expansion are negligible if the pulse duration is in the ps-range. For femtosecond pulses however, third-order dispersion has to be taken into account.” inserting $\Delta\beta(\omega)$ and $\beta(\omega)$ into Equation (2.61) and then taking the inverse Fourier transform it by using [30];

$$A(z,t) = \frac{1}{2\pi}\int_{-\infty}^{\infty} \tilde{A}(z,\ \omega - \omega_0)\exp[-i(\omega - \omega_0)t]\,\mathrm{d}\omega \tag{2.64}$$

gives the following equation for $A(z,t)$;

$$\frac{\partial A}{\partial z} + \beta_1\frac{\partial A}{\partial t} + \frac{i\beta_2}{2}\frac{\partial^2 A}{\partial t^2} = i\Delta\beta_0 A \tag{2.65}$$

Finally, we can insert $\Delta\beta_0$ obtained from Equation (2.57) so that;

$$\frac{\partial A}{\partial z} + \beta_1\frac{\partial A}{\partial t} + \frac{i\beta_2}{2}\frac{\partial^2 A}{\partial t^2} + \frac{\alpha}{2}A = i\gamma(\omega_0)|A|^2 A \tag{2.66}$$

The nonlinear parameter γ is described as ;

$$\gamma = \frac{n_2(\omega_0)\omega_0}{cS_{eff}} \tag{2.67}$$

where the effective area S_{eff} can be found from the modal distribution function of an optical fiber. Note that if is approximated by a Gaussian function, then effective area is simply $S_{eff} = \pi w^2$. Typically, S_{eff} ranges between 1-100 μm^2 in the 1.5 μm region.

The Equation (2.66) can further be simplified by a coordinate transformation. If the retarded time is used instead of the proper time [30];

$$\frac{\partial A}{\partial z}+\frac{i\beta_2}{2}\frac{\partial^2 A}{\partial T^2}+\frac{\alpha}{2}A=i\gamma(\omega_0)|A|^2A \tag{2.68}$$

where $T=t-\frac{z}{v_g}\equiv t-\beta_1 z$.

“Because of the resemblance of this equation it is called the nonlinear Schrödinger equation (NLSE) and is used to describe the propagation of ps-range pulses through optical fibers, taking into account chromatic dispersion by β_2, fiber losses by α and fiber nonlinearities by γ”.[29]

“It is useful to introduce two length scales, *dispersion length* L_D and *nonlinear length* L_{NL}. This makes it possible to compare the relative strengths of effects over the propagation distance. These *lengths* are defined as” [30];

$$L_D=\frac{T_0^2}{\beta_2},\qquad L_{NL}=\frac{1}{\gamma P_0} \tag{2.69}$$

Here T_0 is the initial pulse length and P_0 is the pulse peak power. Rewriting equation 2.68 with these new parameters leads to [30];

$$\frac{\partial a}{\partial z}+\frac{i}{2}\frac{L}{L_D}\frac{\partial^2 a}{\partial \tau^2}+\frac{\alpha}{2}a=i\frac{L}{L_{NL}}|a|^2a \tag{2.70}$$

where the absolute square of the field now gives power instead of intensity, through the transformation $a(z,\tau)=A(z,t)/\sqrt{S_{eff}}$.

After this point, we will develop the NLSE a bit more by adding the third-order dispersion (TOD) term, which becomes significant for extremely short pulses (<100 fs). In addition, the spectrum of a short pulse can be wide enough that the Raman scattering will transfer energy from high to low frequency components within the pulse, which is called the self-frequency shift. The next few pages in this section will deal with the extension of the NLSE to include these effects.

“For pulses with a wide spectrum, the Raman effect can amplify low-frequency components of a pulse by energy transfer from the high-frequency components of the same pulse. As a result of it, a red-shift of the optical spectrum of the pulse, a feature referred to as *Raman-induced frequency shift* takes place. To include this effect, one needs to re-evaluate the nonlinear polarization as given in equation (2.40). Any $\chi^{(2)}$ related effects are still neglected, as they require phase matching. The scalar form of nonlinear polarization is given by” [30];

$$P_{NL}(\boldsymbol{r},t)=\frac{3\varepsilon_0}{4}\chi^{(3)}_{xxxx}E(\boldsymbol{r},t)\int_{-\infty}^{t}R(t-t_1)|E(\boldsymbol{r},t_1)|^2dt_1 \tag{2.71}$$

including the delayed response of the polarization by the response function $R(t)$ such that $\int_{-\infty}^{\infty}R(t)dt=1$. After some calculations, the following result can be obtained [30];

$$\frac{\partial A}{\partial z}+\frac{\alpha}{2}A+\frac{i\beta_2}{2}\frac{\partial^2 A}{\partial t^2}-\frac{\beta_3}{6}\frac{\partial^3 A}{\partial t^3}=i\gamma\left[|A|^2A+\frac{i}{\omega_0}\frac{\partial}{\partial T}(|A|^2A)-T_RA\frac{\partial|A|^2}{\partial T}\right] \quad (2.72)$$

where T_R is the first moment of the nonlinear response function given by $T_R=\int_{-\infty}^{\infty}tR(t)dt$. The term β_3 with is responsible for third-order dispersion, ω_0^{-1} term is for self-steepening and shock formation and T_R is for the self-frequency shift. Experimentally, it was found that $T_R=3\,fs$ around 1.5 μm wavelength.

There is a simple solution to this equation if β_2. is assumed to be negative (i.e. anomalous dispersion). This solution is called as “soliton”, which was first observed in 1834 by Scott Russell in water waves propagating with undistorted phase over several kilometers through a canal [42]. Assuming no losses, Equation (2.68) can be written in the following form

$$\frac{\partial A}{\partial z}=i\gamma(\omega_0)|A|^2A-\frac{i\beta_2}{2}\frac{\partial^2 A}{\partial T^2} \quad (2.73)$$

Here, we are searching a solution such that it will preserve its shape while propagating through the fiber. After some calculations, it can be verified that a hyperbolic secant function satisfies this condition: [30];

$$|A(t)|=\sqrt{\frac{|\beta_2|}{\gamma T_0^2}}\,\mathrm{sech}\left(\frac{T}{T_0}\right) \quad (2.74)$$

2.5 Amplification in Rare-Earth Doped Fibers

Optical gain through stimulated emission is a key ingredient of any laser. By doping the core of a fiber with suitable types of atoms, it is possible to obtain lasing at selected wavelengths. For certain applications like medicine, metrology, etc. where the eye-safe region (1.4-2.1 μm) is preferred, dopants such as erbium (1.5 μm), thulium (1.9 μm) and holmium (2.1 μm) are suitable. However, if pure power is required such as in material processing, the most suitable dopant is ytterbium (1.06 μm) because of its small quantum defect. Also Yb ions have a single excited state, which means it is relatively immune to excited state absorption and self-quenching, thus Yb can be doped in higher concentrations. Depending on the energy levels of the dopants, lasing schemes can be classified as a three-level (like Yb) or four-level (like Er) scheme (Fig. 2.8). In either case, dopants absorb pump photons to reach an excitation stage and then relax rapidly into a lower-energy excited state. The lifetime of this intermediate state is usually long (~1 ms for Yb, 10 ms for Er), and the stored energy is used to amplify incident light through stimulated emission. The difference between the three and four-level lasing schemes is the energy state to which the dopant relaxes after a stimulated-emission event. For a three-level case, the dopant ends up in the ground state, whereas for a four-level case, it ends up in an excited state.

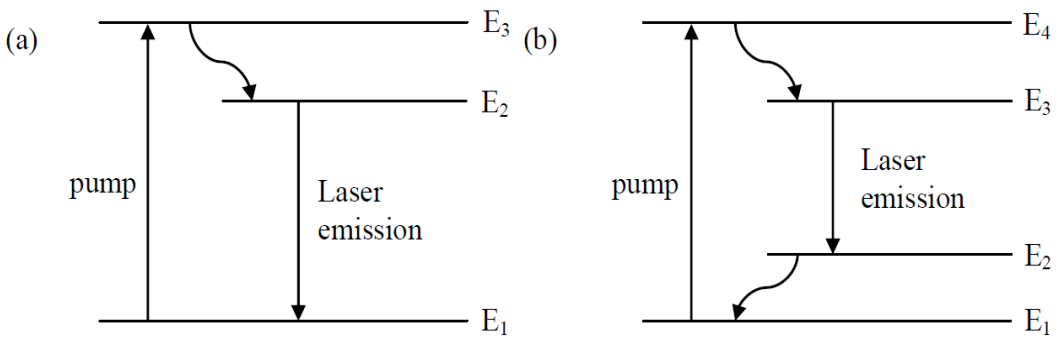

Figure 2.8 Energy-level diagram of three and four level lasing model.

Optical pumping creates the necessary population inversion between the excited and lower energy states and provides the optical gain as given by [32]

$$g(\omega) = \frac{g_{ss}}{1 + \frac{\tau P}{E_{sat}}} = \frac{g_{ss}}{1 + \frac{P}{P_{sat}}} \tag{2.75}$$

where g_{ss} is the small signal gain at the peak of the gain spectrum, ω is the frequency of the incident signal, and P is the optical power of the signal being amplified, P_{sat} is the saturation power, E_{sat} is the saturation energy, τ is the gain relaxation time.

The actual gain spectrum of a fiber laser can deviate significantly from the Lorentzian profile. The shape and the width of the gain spectrum are sensitive to core composition (i.e. the amorphous nature of the silica and the presence of other co-dopants such as aluminum or germanium). The measured absorption and emission spectrums of a Yb-doped silica fiber can be seen in Fig. 2.9.

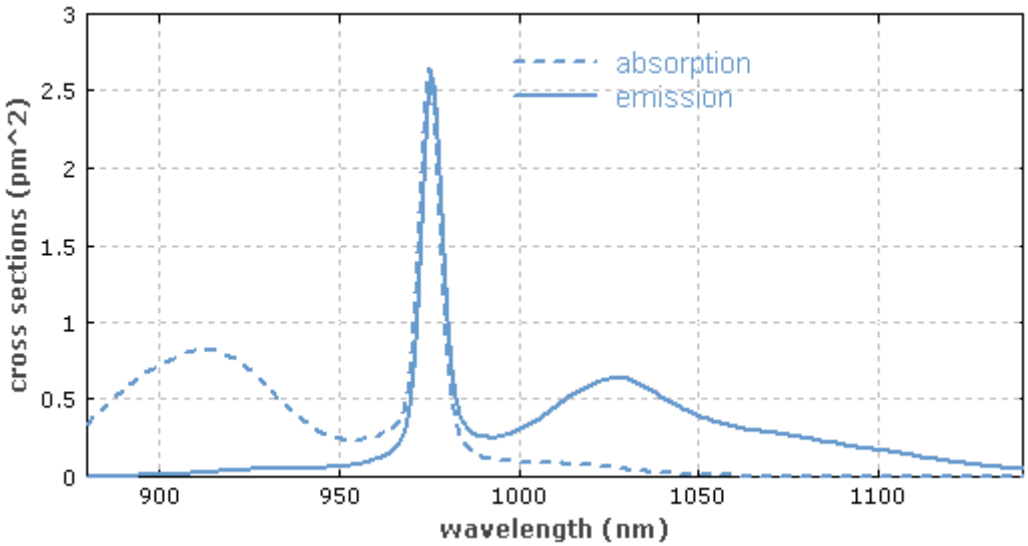

Figure 2.9 Absorption and emission cross section of Yb-doped silica glass [34].

Incorporating the gain term into the NLSE given by Eq. 2.68 is not an easy task, however comprehensive theoretical background and detailed derivation can be found in [32, 33] .There is more than one possible approach to modeling this effect, but a reasonably broadly applicable, yet simple result is given by

$$\frac{\partial a}{\partial z}+\frac{i}{2}(\beta_2+igT_2^2)\frac{\partial^2 a}{\partial T^2}+\frac{\alpha-g}{2}a = i\gamma(\omega_0)|a|^2 a \qquad (2.76)$$

where $T=t-\beta_1 z$ is the reduced time. The T_2 term accounts the decrease in gain for spectral components of the pulse far from the gain peak. Note that the gain is simply added near the loss term with the inverse sign. However, the dispersion term is slightly modified by the "gain dispersion", which is caused by the finite gain bandwidth of the doped fibers. This equation, with the addition of saturable absorption (of the form $|a|^2 a$) would constitute the so-called "master equation of mode-locking" [35].

2.6 Mode Locking Theory

"Mode-locking a laser leads to ultra-short pulses with duration of a few-ps or less. For this purpose a phase relation between the many longitudinal modes which can exist in a laser cavity should be found. In this section, the principle of only passive mode-locking will be introduced using an artificial saturable absorber, as this is the method implemented in the ytterbium-doped fiber laser used in this thesis. This subsection is based on [36, 40] and comprehensive theoretical background and detailed derivation can be found in these references."

Mode-locking is, in simplified terms, to induce a fixed phase relationship between the longitudinal modes of a resonant cavity. There can be many modes in a ring cavity, which satisfy;

$$n\lambda_n = 2L \qquad (2.77)$$

where L is the length of the ring cavity, n is the mode number and λ_n is the corresponding wavelength. Interference between these modes produces pulses, which can be as short as femtoseconds depending on the number of the modes involved. Of course this is related to spectral width of the pulse as it can be seen from the relation above. The total electric field in the cavity can be written in terms of the fields of separate modes as;

$$E(z,t)=\sum_n E_n(z,t)=\sum_n E_{0,n}\, e^{ik_n z-i\omega_n t}, \qquad E_{0,n}=\left|E_{0,n}\right|e^{i\phi_n} \qquad (2.78)$$

where $E_{0,n}$ is the complex amplitude of the n-th mode and ϕ_n is the phase. For simplicity let's assume the amplitude of all modes are the same (i.e. square shaped spectrum). Then we can write the intensity as;

$$I(z,t)\propto E(z,t)E^*(z,t)=|E_0|^2\sum_{n=1}^{N}\sum_{m=1}^{N} e^{i(\phi_n-(\phi_m)}(m-n)\Omega\left(\frac{Z}{c}-t\right) \qquad (2.79)$$

where the frequency difference between two consecutive modes is defined as

$$\Omega = \omega_{n+1} - \omega_n = \frac{\pi c}{L} \tag{2.80}$$

For the mode-locking condition, all of the modes should have a fixed phase relation. Then we can write the intensity in a simpler way;

$$I(z,t) \propto E(z,t)E^*(z,t) = |E_0|^2 e^{i\delta\phi} \sum_{n=1}^{N} \sum_{m=1}^{N} e^{i(m-n)\Omega\left(\frac{z}{c}-t\right)} \tag{2.81}$$

The term in the summation will be equal to unity for the following condition:

$$\Omega\left(\frac{z}{c} - t\right) = 2\pi j \quad \leftrightarrow \quad z - ct = 2Lj, \;\; j = 0,1,2,\dots \tag{2.82}$$

where j is an integer. In this case, the intensity is the maximum, which means that a pulse is formed with;

$$I_{max} = N^2|E_0|^2 \equiv N^2 I_0 \tag{2.83}$$

The temporal and spatial separation of neighboring pulses can be derived from Equation (2.84) as;

$$\Delta z = 2L, \quad \Delta t = \frac{2L}{c} \equiv T \tag{2.84}$$

This means the intensity maxima repeat with the roundtrip time T of the laser resonator and there is only one maximum inside the cavity at any time. The peak of the pulses is proportional to N^2. We can also calculate full-width-half-maximum (FWHM) of the pulses; the superposition of N modes is assumed to be similar to the interference of N planar waves at a fixed time $= 0$. Using geometric series;

$$I(t) = I_0 \frac{\sin^2\left(\frac{N\Omega}{2}t\right)}{\sin^2\left(\frac{\Omega}{2}t\right)} \tag{2.85}$$

The FWHM of the pulses can be derived from the above equation, which yields a pulse width decreasing with the number of modes, as expected;

$$I(\Delta T) = \frac{1}{2} I_{max} \quad \rightarrow \quad \Delta T = \frac{1}{N}\frac{2L}{c} = \frac{1}{N}T \tag{2.86}$$

The fixed phase relation between the superposed modes can be achieved by creating a modulated gain (or loss) in the cavity with frequency Ω. All the techniques for mode-locking rely on this principle. Due to this modulation, the electromagnetic field in the cavity gets additional time dependence;

$$E_n(z,t) = (E_{0,n} + E_n^{mod}\cos\Omega t)e^{ik_n z - i\omega_n t} \tag{2.87}$$

$$= \left[E_{0,n}e^{-i\omega_n t} + \frac{1}{2}E_n^{mod}(e^{-i\Omega t} + e^{i\Omega t})e^{-i\omega_n t}\right]e^{ik_n z}$$

$$= \left[E_{0,n}e^{-i\omega_n t} + \frac{1}{2}E_n^{mod}(e^{-i\omega_{n+1} t} + e^{-i\omega_{n-1} t})\right]e^{ik_n z}$$

From this equation, it can be seen that the time dependence in every mode induces sidebands whose frequencies coincide with the frequencies of neighboring modes. Since this is valid for the total bandwidth, phase synchronization, so called “mode-lock”, between all longitudinal modes is achieved. There are several methods to create the desired gain or loss modulation in the resonator in order to achieve mode-locking, but in general giving loss is the easier and preferred one. These methods are mainly divided into two subgroups; active and passive mode-locking. For active mode-locking, generally (acousto-optic or electro-optic) modulators are utilized, while for passive mode-locking, saturable absorbers are used. As a saturable absorber, usually nonlinear polarization evolution (NPE) is used. Since the polarization rotation (due to Kerr effect) at the peak of a pulse will be higher than at the wings, it is possible to selectively pass the peak of the pulse through a polarizer beam cube (PBS) by carefully controlling the polarization so that NPE acts as a saturable absorber. The saturable absorber favors the pulse formation since the phase locked modes experience a lower loss. However, for the relevance of this thesis, only a special case of passive mode-locking will be explained in detail in the subsequent part.

In order to obtain passive mode-locking process (for detail see [41]), the nonlinear element creates mode-locked lasing process more convenient than continuous-wave (cw) lasing process that presents a lower optical efficiency at low power levels so that the short pulse which has higher peak power experiences more net gain.

When the orthogonally polarized elements of one pulse propagate inside an optical fiber, the use of change of intensity dependence in polarization can create mode-locked fiber lasers. The polarization of the pulse center changes more than the wings of the pulse that has lower intensity.

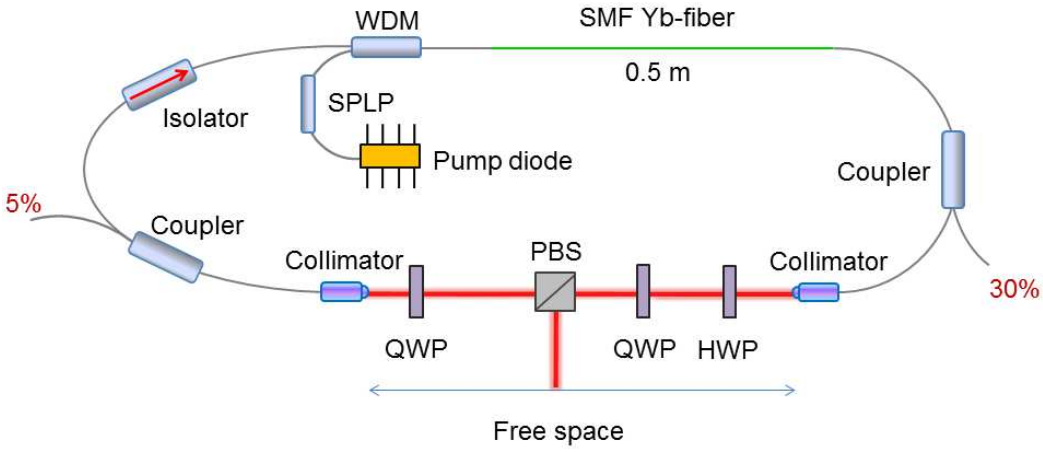

Figure 2.10 Schematic of a fiber ring laser mode-locked via NPE

Mode-locking with the nonlinear polarization evolution process might be realized when one think about the concept of ring fiber configuration as shown in Figure 2.10. After passing through the polarizing beam splitter (PBS), the polarization state of the pulse is linear. The pair of polarizing beam splitter and quarter-wave plate creates slightly elliptical polarization state just before entering the optical fiber. When the pulse propagates in the fiber, Kerr effect nonlinearly manipulates the polarization state of the pulse. After the optical fiber segment, the change of polarization state will be maximum at the center of the pulse. After passing through the pair of quarter and half wave plate, the polarization state of the pulse center will be linear, "so the center of the pulse passes through the PBS cube and the wings are reflected out of the cavity through the nonlinear polarization evolution (NPE) port." The total overall influence of the waveplates, PBS cube and fiber segment is shortening of the pulse after each round trip, with the PBS effectively acting as a saturable absorber.

2.7 Main Limitations for Fiber Laser Oscillators and Amplifiers

In this section, we will present the factors that mainly limit the high power designs. In fiber lasers, light is strictly confined in the core region and propagates for long distances (several meters) in a nonlinear medium compared to other solid state lasers. So it is understandable that the nonlinear effects are the main concerns in high power fiber laser design, coming before the material damage or thermal problems.

Stimulated Raman scattering (SRS) is the most important nonlinear effect, which severely limits the performance of a high power system. As explained before, SRS involves conversion of an incident photon to a lower energy scattered photon and an optical phonon. This effectively extracts energy from the main pulse and generates a Stokes wave at a downshifted frequency. The basic equation governing the Raman process is [30]

$$\frac{dI_s}{dz} = g_R(\Omega) I_p I_s \tag{2.88}$$

Where I_s is the Stokes intensity, I_p is the incident pump intensity, and is g_R the Raman gain coefficient, which is a function of the frequency difference Ω between the pump and Stokes waves. Raman gain coefficient is fundamentally related to the imaginary part of the third-order susceptibility $X^{(3)}$. Fig 2.11 shows the Raman gain spectrum for silica as a function of Ω.

For silica, the Raman spectrum is a continuum because of its amorphous structure unlike many media where the Raman shift occurs in specific frequencies. The peak of the Raman gain, 10^{-13} m/W, occurs around 13.2 THz. This means that for a 1060 nm pump wavelength, the peak of the Stokes wave will be around 1120 nm. If we integrate Eq. 2.88, we get [30]

$$I_s = I_s(0)\exp(g_R I_p L) \tag{2.89}$$

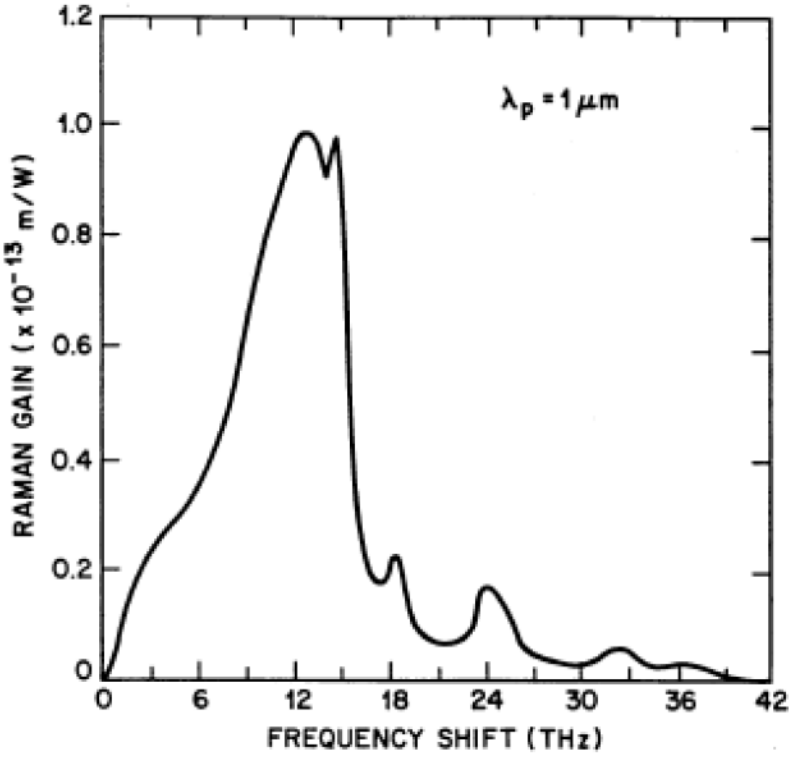

Figure 2.11 Raman gain spectrum for silica at 1 μm wavelength [30].

From here we can deduce two important results. First, the Stokes wave grows exponentially with the pump intensity and the length of the fiber *L*, hence so at some point SRS will set a fundamental limit to the achievable power of the system. Second, Stokes wave needs an initial intensity $I_s(0)$ in order to be strengthened. If there is no signal in Stokes frequency, it will grow from the quantum fluctuations in the cavity. Assuming a single photon in each mode of the cavity, the following relation can be obtained [30]:

$$\frac{g_R P_{cr} L}{A_{eff}} \cong 16 \tag{2.90}$$

Here P_{cr} is the critical incident pump power where the Raman threshold is reached and defined as the power at which the Stokes power becomes equal to the pump power at the fiber output.

Another important effect not describe previously is stimulated Brillouin scattering (SBS), and it is similar to SRS. It is also related to the third-order susceptibility $X^{(3)}$ and can be effective at very low powers if the conditions are suitable. SBS is basically conversion of an incident photon to a scattered photon with slightly lower energy and an acoustic phonon. Due to the phase-matching requirements, the scattered photon travels in the opposite direction of the incident photon. For silica, this is on the order of 10 GHz with a bandwidth of 10 MHz. It is also possible to write an equation for the Brillouin threshold similar to Eq. 2.90 [30],

$$\frac{g_B P_{cr} L}{A_{eff}} \cong 21 \tag{2.91}$$

where g_B is the Brillouin gain with a peak value of .5x10^{-11} m/W This is a relatively larger value compared to the Raman gain indicating a smaller onset time for SBS. However, because of its small bandwidth, SBS can only be effective for very narrow-spectrum pulses like the ones form a single-frequency laser. For pulses shorter than 10 ns, SBS is negligible. Also, there are some techniques to suppress SBS. Since it is sensitive to the phonon velocity, nonuniform heating of the fiber throughout its length will help by changing the phonon velocity. Actually, in an amplifier this is the case; the entrance of the fiber where the pump light is injected has significantly higher temperature than the output end.

Bulk material damage threshold of silica is one of the important parameters to keep in mind while designing a high power fiber laser. In literature, one can find many values for this threshold. Also, pulse duration and doping level have effects on this value, which makes things more complex. In general, it is safe to assume a value of 100 GW/cm^2 for a 1 ns-long pulse, which is inversely proportional to the square root of the pulse duration. For CW operation, the damage threshold approaches to 10 GW/cm^2. For doped fibers half of these values should be used.

Surface damage threshold of silica is much smaller than the bulk damage threshold. Again, there is no agreement about its value however taking it as five times smaller than the bulk damage threshold is a reasonable estimate. This means that the fiber ends are much more sensitive to optical damage than the bulk fiber itself. In high power designs, it is customary to use end-caps in order to increase this threshold level.
Self-focusing is a phenomena occurring at extremely high powers. The guided light focuses onto itself because of the index profile created by the intense electric field. The critical power can be estimated from [30]

$$P_{cr} \cong \frac{0.15\lambda^2}{n_0 n_2} 16 \tag{2.92}$$

where $n_0$is the refractive index and n_2 is the nonlinearity coefficient. For silica, the critical power for self-focusing is around 4.5 MW at 1 μm wavelength.
Core fusing (or fiber fusing) is a catastrophic damage induced by a defect point, which can occur at power levels as low as few watts. This defect point can be inside the core as well as a dust particle at the tip of a fiber. At this point, a hot plasma forms and travels in the backward direction with a relatively slow speed (~1 m/s), even detectable by eye. It is especially dangerous in telecommunication systems where kilometers of fiber may be destroyed by this process. It is also important for the high power systems since it is an unpredictable event, which may damage the other parts of the system.

Finally, photodarkening is the increase of optical losses by formation of color centers. Although the absorption occurs mainly in the visible region, its extension into the infrared region may severely drop the performance of fiber lasers operating in the 1-2 μm band. The formation of color centers becomes easier in the presence of large diameter atoms (like rare-earth atoms such as Yb) and their number rapidly increases by the collaborative action of excited Yb ions. As a result, lowering the doping level is an efficient way to reduce photodarkening rate. Co-doping with certain ions like phosphorus also helps. Photodarkening is a reversible process that can be cured by annealing the fiber at ~300 ºC but the coating will be destroyed during this process.

CHAPTER 3

NUMERICAL SIMULATIONS

3.1 Method of Numerical Simulation

In this chapter, Method and results of the numerical simulation software which was developed by ultra-fast optic (UFO) group in Bilkent University is explained detail. Theoretical background of the simulation is based on solving nonlinear Schrödinger equation (NLSE) by the *split-step Fourier method.* It includes the effects of second and third-order dispersion, linear losses, saturable gain and nonlinear effects such as gain dispersion, Raman scattering, self-phase modulation, saturable absorption and band-pass filter effects. The initial pulse assumption is to start from noise or a Gaussian profile. The simulation runs over many roundtrips until a steady state solution is reached. NLSE containing all of these effects is shown in equation (3.1)

$$\begin{aligned}&\frac{\partial a}{\partial z}+\frac{i(\beta_2+ig\tau_2^2)}{2}\frac{\partial^2 a}{\partial \tau^2}-\frac{\beta_3}{6}\frac{\partial^3 a}{\partial \tau^3}+\frac{\alpha-g}{2}a\\&=i\gamma\left[|a|^2 a+\frac{i}{\omega_0}\frac{\partial}{\partial \tau}(|a|^2 a)-T_R a\frac{\partial |a|^2}{\partial \tau}\right]\end{aligned} \tag{3.1}$$

Two newly defined operators are introduced in order to make this equation more convenient;

$$\frac{\partial a}{\partial z}=(\hat{D}+\hat{N})a \tag{3.2}$$

where the differential operator (D) represents the linear dispersion and absorption terms and the nonlinear operator (N) represents all nonlinear effects during pulse propagation. These two operators are defined by;

$$\hat{D}=\frac{i(\beta_2+ig\tau_2^2)}{2}\frac{\partial^2 a}{\partial \tau^2}-\frac{\beta_3}{6}\frac{\partial^3 a}{\partial \tau^3}+\frac{\alpha-g}{2} \tag{3.3}$$

$$\hat{N}=i\gamma\left[|a|^2 a+\frac{i}{\omega_0}\frac{\partial}{\partial \tau}(|a|^2 a)-T_R a\frac{\partial |a|^2}{\partial \tau}\right] \tag{3.4}$$

The split-step method assumes that the fiber is divided into small pieces of fiber, each with length h. The approximate solution of the split-step Fourier method is reached by assuming that pulse propagation over small pieces is achieved in three steps. First, the pulse propagates over half the distance with only dispersive effects. Then, in the middle of

the section, nonlinearity is applied after which the pulse propagates again half the distance with only dispersive effects (Fig. 3.1).
Mathematically,

$$a(z+h,\tau) \cong \exp(\frac{h}{2}\hat{D})\exp(h\hat{N})\exp(\frac{h}{2}\hat{D})a(z,\tau) \tag{3.5}$$

The terms with can be evaluated in Fourier domain much more easily:

$$\exp(\frac{h}{2}\hat{D})a(z,\tau) = F_T^{-1}\exp\left(\frac{h}{2}\hat{D}(i\omega)\right)F_T a(z,\tau) \tag{3.6}$$

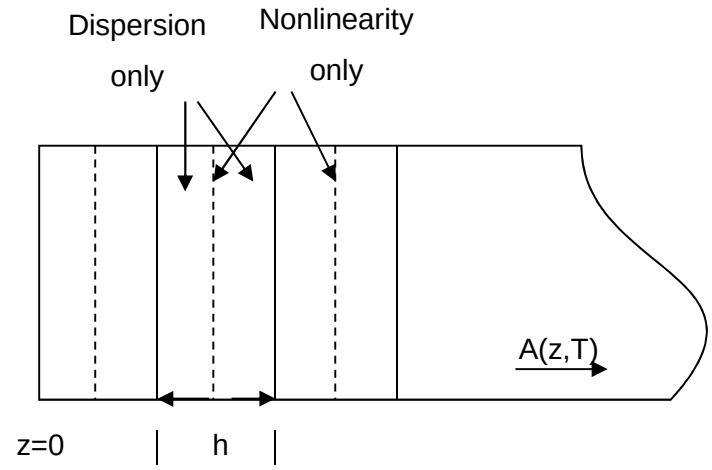

Figure 3.1 illustration of split-step Fourier method used for numerical simulations

where F_T denotes the Fourier transform operation. Since *D(iω)* is just a number in the Fourier space, the evaluation of Eq (3.5) is straightforward. This is why the split-step Fourier method is order of magnitude faster than methods like finite difference.

A screenshot of the simulator interface is shown in Fig. 3.2. The parameters to be entered into the simulator are listed in Table 3.1. “The initial pulse shape can be one of the pre-defined pulse shapes ranging from Gaussian pulse shape to noise. Each segment of the laser cavity should be configured separately. The saturable absorber (SA) is implemented at the end of a segment, by converting the total nonlinear phase shift accumulated over the round trip into an amplitude modulation. The semiconductor and NPE saturable absorbers are modeled in the simulation as”

$$I_{SSA} = 1 - \frac{q}{1 + I/I_{sat}} \tag{3.7}$$

$$I_{NPE} = 1 - q\cos^2\left(\frac{\pi}{2}\frac{I}{I_{sat}}\right) \tag{3.8}$$

where and are the intensities before and after SA, is the modulation depth and is the saturation intensity of the SA. Gain saturation is also taken into account as

$$g(E) = \frac{g_{ss}}{1 + \frac{1}{E_{sat}}\int |a|^2 \, d\tau} \tag{3.9}$$

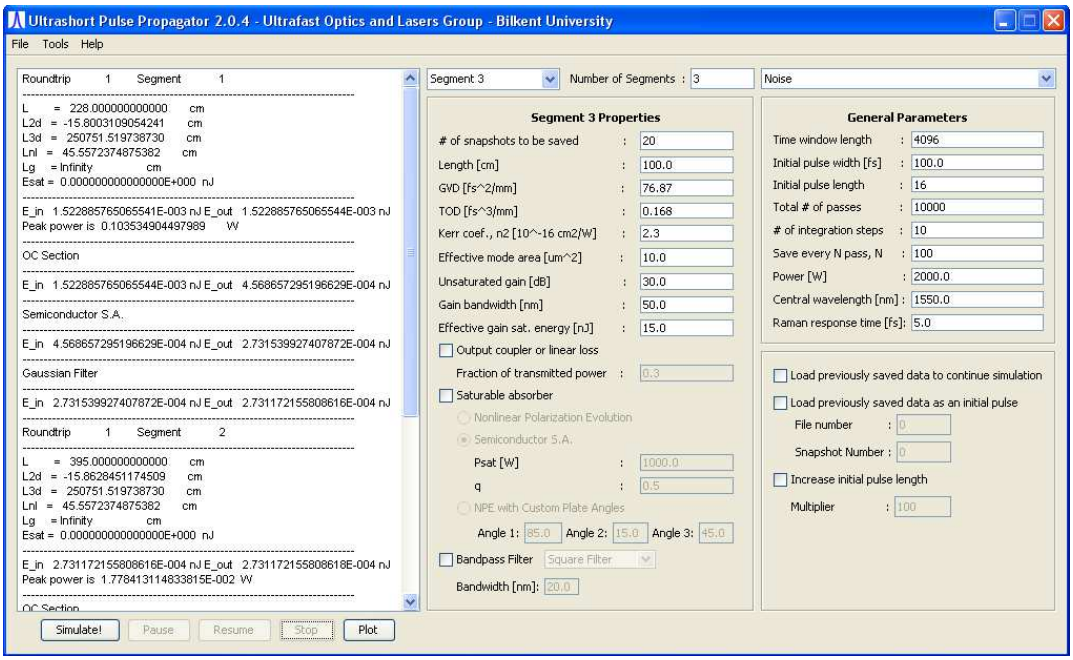

Figure 3.2 Screenshot of the simulator user interface

Table 3.1 Numerical parameters needed for the simulator

Parameter	Function
Time window length	Number of data points for discretizing time
Initial pulse width [fs]	Actual length of the pulse corresponding to a # of data points
Initial pulse length	# of discrete points representing the FWHM of initial pulse
Total # of passes	# of passes to be made over the entire sequence of segments
# of integration steps	# of discrete steps taken per each page per segment
Save every N pass, N	# of roundtrips after which data is saved to file
Power [W]	Actual power corresponding to unit size of power
Central wavelength [nm]	The central wavelength of the light used for simulation
Raman response time [fs]	Parameter characterizing the strength of the Raman effect
# of snapshots to be saved	# of segments each fiber section is divided into
Length [cm]	Physical length of the segment
GVD [fs^2/mm]	Second order dispersion parameter
TOD [fs^3/mm]	Third order dispersion parameter
Kerr coef., n_2 [10^{-16}cm2/W]	The Kerr nonlinearity coefficient
Effective mode area [μm^2]	Effective mode area for the propagating beam
Unsaturated gain [dB]	Small signal gain of the amplifier
Gain bandwidth [nm]	Finite gain bandwidth for parabolic approximation
Effective gain sat. energy	Saturation energy in arbitrary units for the gain
Output coupler /linear loss	Adds an output coupler to the end of the segment

3.2 Results of Numerical Simulation

The study of numerical simulations are conducted to obtain information about the dynamic properties of the pulse throughout the laser cavity, beginning with fiber laser oscillator, fiber stretcher, preamplifier and power amplifier. The simulation was done with two parts. In the first part, we simulate oscillator that is responsible for pulse generation and in the second part, the simulation run for pulse propagation outside the oscillator. After obtaining pulse characteristics of the oscillator from the simulation, this simulation result was used as the initial condition for the pulse propagation outside the oscillator such as fiber stretcher, the preamplifier and the power amplifier.

The subsequent parameters used for the oscillator fiber segments: $\beta_2 = 24.18\ fs^2/mm$, $\beta_3 = 76.32\ fs^3/mm$, $n_2 = 2.3\ x\ 10^{-16}\ cm^2/W$. The effective mode area for the single mode fiber and gain fiber was 25 μm^2 and 23 μm^2 respectively. For the oscillator simulation scenario, there are three main section which are the in-fiber propagation, saturable absorber that describes NPE and a Gaussian-shaped band-pass filter with 10 nm bandwidth (both of which are modeled as transfer functions, in time and frequency domains, respectively). The numerical Simulations are conducted until the laser cavity reaches a stable solution within certain number of round trips. The numerical result was checked by increasing the sampling resolutions. The following figures 3.3 and 3.4 display the simulation results for the oscillator with total cavity GVD of 0.16 ps^2, $E_{sat} = 1.1\ nj$ and $g_0 = 30\ dB$. Besides, the simulation results of the fiber stretcher and power amplifier are shown in figures 3.5 – 3.8. The lengths and positioning of the fibers are as used in the experiments. The combined action of gain, nonlinearity, normal dispersion, and spectral filtering leads to linearly chirped optical pulses with a spectral profile that develops the steep and structured edges characteristic of self-phase modulation (SPM).

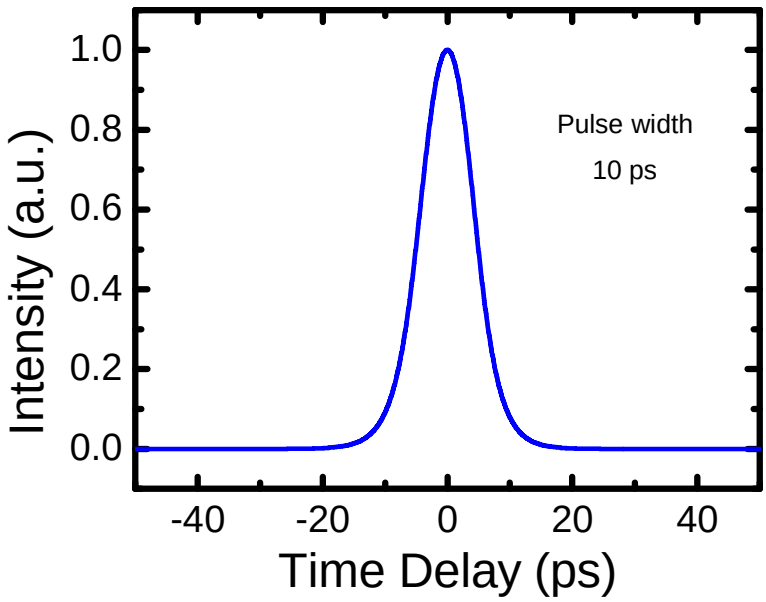

Figure 3.3 The simulation result of pulse width the oscillator output.

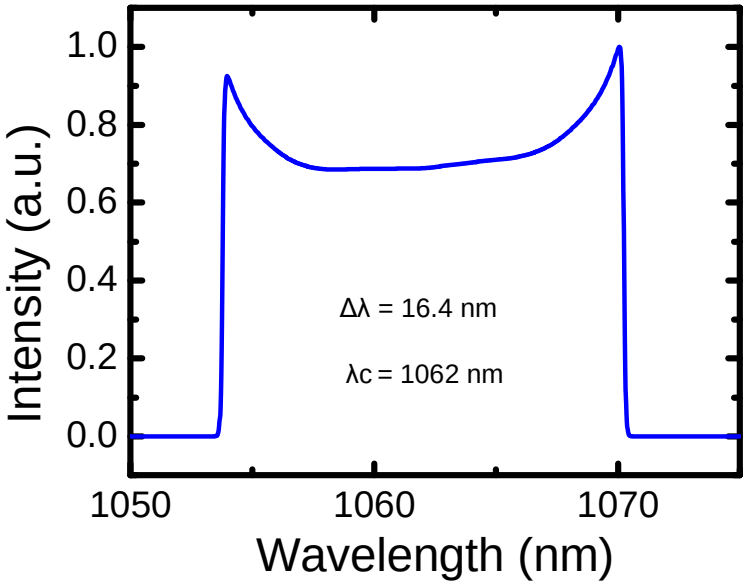

Figure 3.4 The simulation result of the oscillator output spectrum

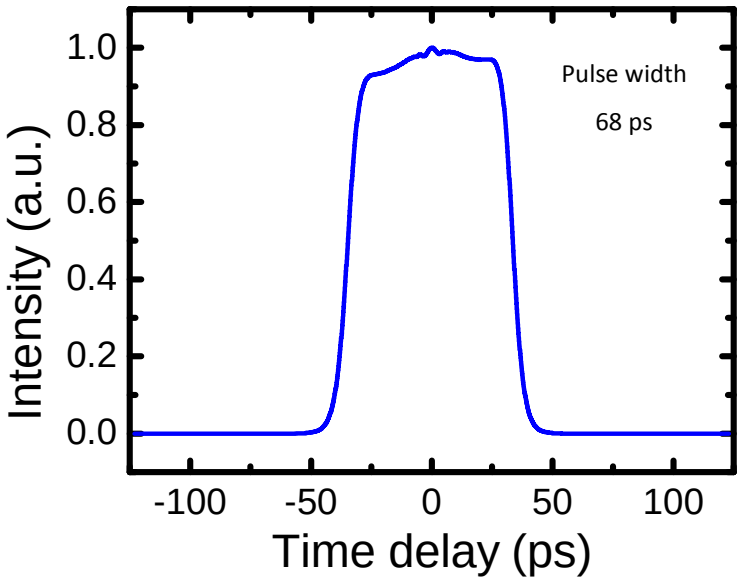

Figure 3.5 The simulation result of pulse width of the fiber stretcher.

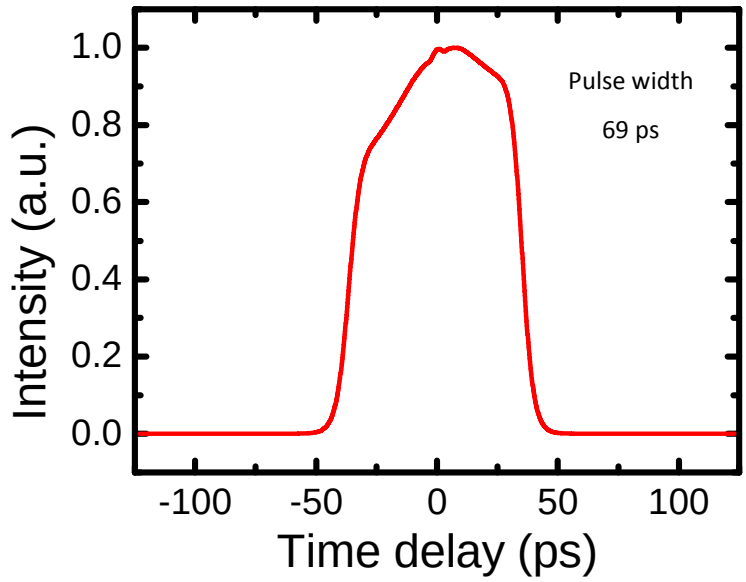

Figure 3.6 The simulation result of pulse width of the power amplifier

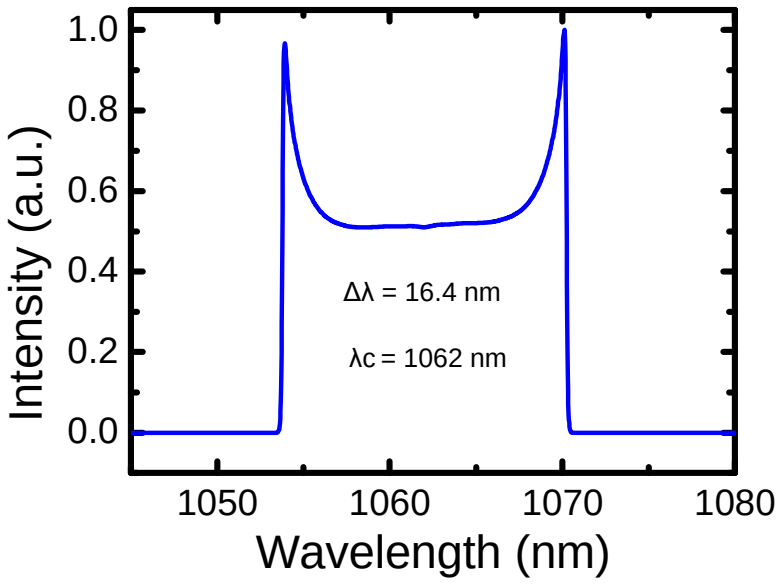

Figure 3.7 The simulation result of the fiber stretcher output spectrum.

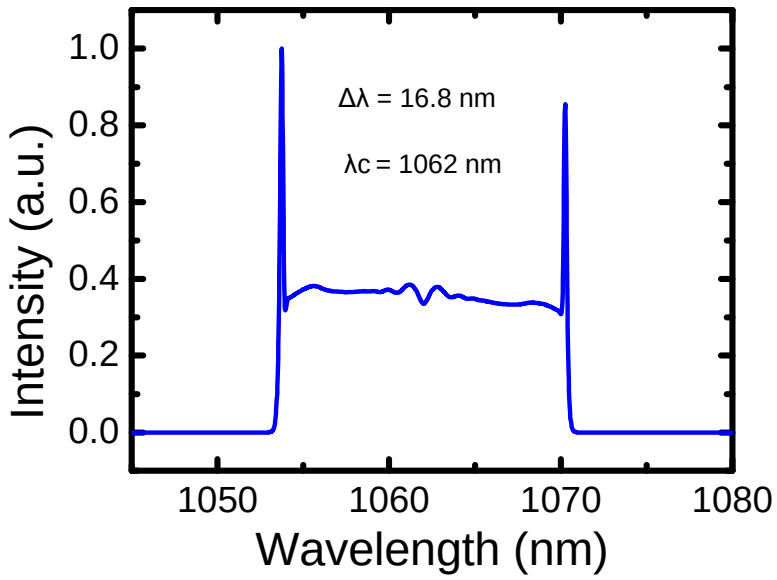

Figure 3.8 The simulation result of the power amplifier output spectrum.

CHAPTER 4

DESIGN AND IMPLEMENTATION OF FIBER LASER SYSTEM

In this chapter, design and implementation studies will be explained during the development of this fiber laser system. The laser system used for this study is based on a MOPA (master oscillator power amplifier) configuration. The basic idea behind the MOPA is that a fiber laser system is divided into a seed laser and a laser amplifier which increases the output power. In the first part of this chapter, the seed laser is explained and in the second part the amplification system will be described in detail.

4.1 Seed Laser Source

Short-pulse, high-power fiber lasers has been used in many areas such as scientific, biomedical and industrial, applications. “Especially, the use of short-pulsed fiber lasers in material processing is promising due to their simplicity, low cost and ease of use. For precision micromachining, surface texturing, pulsed laser deposition, and marking, typically relatively low power (<20 W) pulsed fiber lasers are utilized. The pulse durations and repetition rates range from 100 fs to 100 ns and from 20 kHz to 100 MHz, respectively” [46].

The purpose behind the development of this laser is precision micromachining. This purpose gives the initial point for determining some laser parameters such as pulse duration, pulse energy and repetition rate. It is well-known that nanosecond pulsed lasers are not appropriate for precision micromachining because of excessive thermal damage to the material [43-45]. For these applications lasers typically have pulse energy on the order of a few mJ and repetition rate in the kHz range. From references [43-45] point of view, the desired seed source parameters are determined to within picosecond pulse duration and MHz repetition rate. . As a result, the seed laser is chosen as a passively mode locked laser oscillator with nonlinear polarization evolution (NPE) these lasers typically have lower energy per pulse and higher repetition rates than nanosecond lasers have.

4.2 Passively Mode Locked Laser Oscillator

The diagram of the implemented experimental setup for the seed source is shown in Fig. 4.1. The seed source is an all-normal dispersion (ANDi) type Yb-doped fiber oscillator which is a passively mode locked laser with an artificial saturable absorber. Nonlinear polarization evolution (NPE) method is used as the saturable absorber in the oscillator. NPE part of the oscillator is labeled as ‘Free space’ in Fig. 4.1. The main idea is based on the fact that the polarization of the pulse center changes more than the wings of the pulse that has lower intensity.

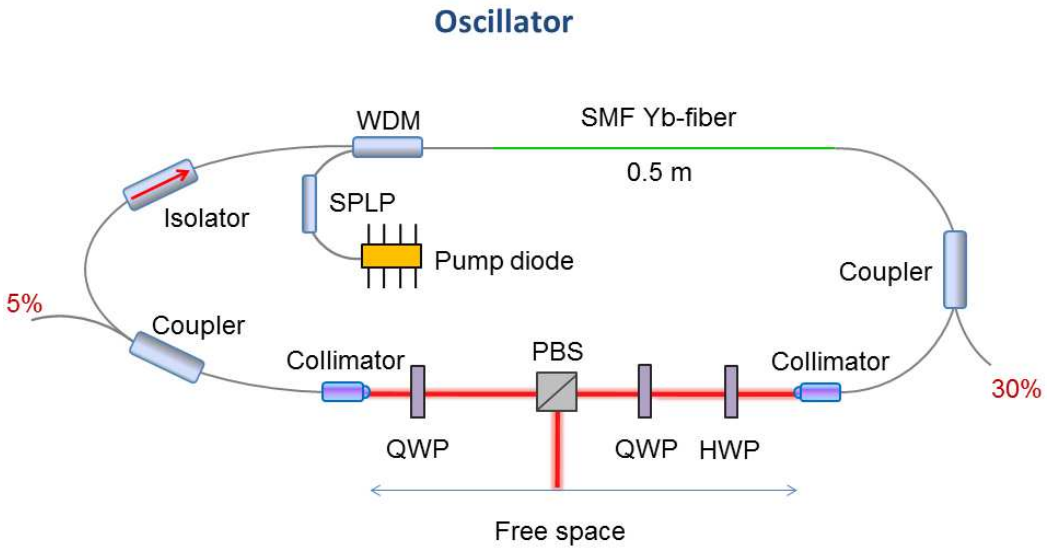

Figure 4.1 Diagram of the fiber laser oscillator: PBS: polarizing beam splitter cube, SMF: single-mode fiber, SPLP: single-mode pump protection, WDM: wavelength-division multiplexer, QWP: quarter wave plate, HWP: half wave plate

.

The pulse shaping mechanism with NPE is briefly explained as follows: After passing through the polarizing beam splitter (PBS), the polarization state of the pulse is linear. The pair of polarizing beam splitter and quarter-wave plate creates slightly elliptical polarization state just before entering the optical fiber. When the pulse propagates in the fiber, Kerr effect nonlinearly manipulates the polarization state of the pulse. After the optical fiber segment, the change of polarization state will be maximum at the center of the pulse. After passing through the pair of quarter and half wave plate, the polarization state of the pulse center will be linear, “so the center of the pulse passes through the PBS cube and the wings are reflected out of the cavity through the nonlinear polarization evolution (NPE) port.” The total overall influence of the wave plates, PBS cube and fiber segment is shortening of the pulse after each round trip, with the PBS effectively acting as a saturable absorber.

The oscillator consists of 4.8 m of standard single-mode fiber (SMF) for 1 μm wavelength (core diameter of 6.2 μm, 0.14NA) and 0.5 m of highly Yb-doped gain fiber (core diameter of 4 μm, 0.14NA, ~1200 dB/m nominal absorption at 976 nm), followed by another 1.5 m of SMF. Together with the fixed length free-space section, this gives a pulse repetition frequency of 30 MHz. The gain fiber is pumped in-core by a fiber-coupled laser diode operating at 976 nm with an approximate output power of 285 mW. In addition to that, single-mode pump protection (SPLP) is added after the pump diode to protect the diode from reflected light. The coupling of pump power to the cavity is done by using a wavelength-division multiplexer (WDM). The total group velocity dispersion (GVD) of the cavity is ~0.16 ps^2. The table 4.1 explains obviously calculation of total GVD of the cavity where β_2 represents the dispersion of group velocity.

Table 4.1 Cavity total GVD calculation table

Fiber type	**Length (cm)**	**β_2 (fs^2/cm)**	**GVD_{total} (fs^2)**
Yb-fiber	50	279.349	13967.45
HI-1060	349	221.478	77295.822
Lucent-980	280	268.24	75107.2
Grating	0	0.0	0
Air	18	0	0
Total	697		166370

Fast saturable absorption required for mode-locking is obtained from nonlinear polarization evolution (NPE), which is implemented with three wave plates and a polarizing beam splitter cube. Also a filter isolator is used with a bandwidth of 10 nm. Due to the heavy chirp on the pulse, the influence of the filter in the time domain is to remove the temporal wings of the pulse, and assist in the saturable absorber. The transmission peak of the isolator, centered at 1062 nm, sets the central wavelength of the pulses. Actually, the optical isolator is placed in the oscillator to maintain unidirectional ring cavity configuration which ensures that the laser signal travels only one direction in ring cavity. In addition, the coupler 95/5 is placed to monitor the oscillator characteristics. The mode-locked operation is self-starting and appears to be stable if the temperature of the environment is stable and there is no external stress on the fiber of the oscillator such as vibration, mechanical shock, etc. An output power of 65 mW is obtained directly through a 30% output coupler after the gain fiber. The detail results and measurement of the oscillator will be shown in following subsections. The photo of the mode locked Yb-doped fiber laser oscillator is displayed in figure 4.2 and figure 4.3.

Figure 4.2 The photo of implemented mode locked Yb-doped fiber laser oscillator.

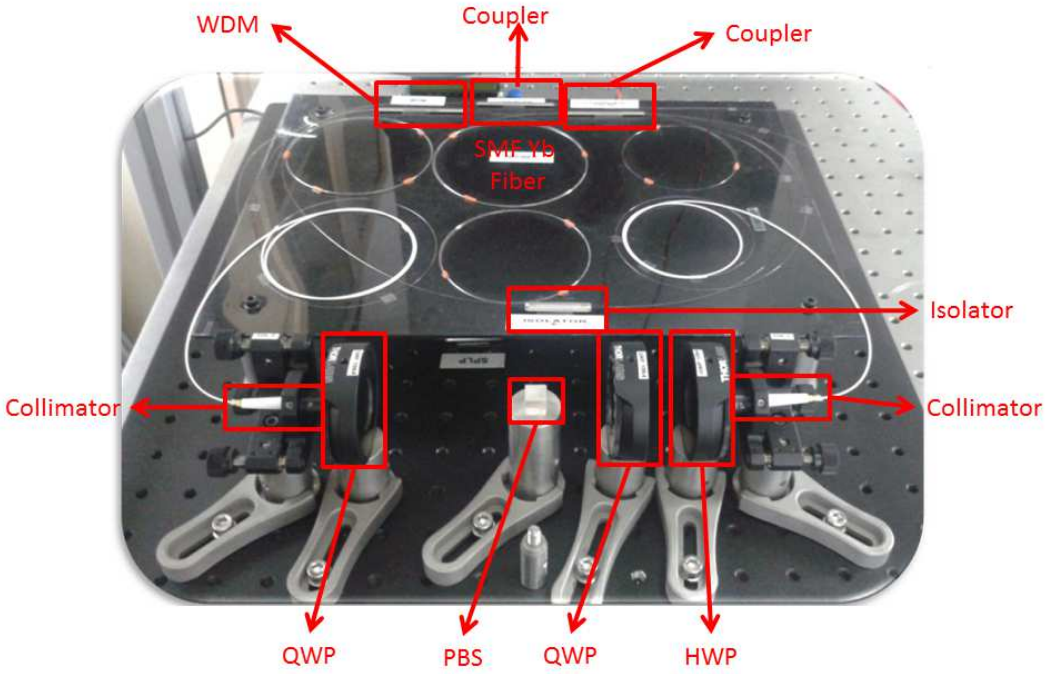

Figure 4.3 The labeled photo of implemented mode locked Yb-doped fiber laser oscillator.

4.3 Oscillator Characterization

4.3.1 Autocorrelation Measurement of Oscillator Pulse

"Characterization of femtosecond laser pulses cannot be performed electronically since oscilloscopes and photo detectors do not have bandwidths on the order of a few hundred THz. For femtosecond pulses, autocorrelation technique has to be performed in the optical domain using nonlinear optical effects".

In this thesis intensity autocorrelation is used for temporal measurement of the pulse. "The technique depends on second-harmonic generation. Fig. 4.4 illustrates the setup of the autocorrelation. Initially the input pulse is split into two, and one of the pulses is delayed by τ. Then the two pulses are focused on a second-harmonic crystal in a non-collinear fashion. Assuming the material response is instantaneous, the convolution of two interfering signals or the induced nonlinear polarization simplifies to"; $P^{(2)}(t) \propto E(t)E(t-\tau)$

$$P^{(2)}(t) \propto E(t)E(t-\tau) \tag{4.1}$$

"Since the photo detector's response is much longer than the pulse width, it integrates the incident light intensity leading to intensity autocorrelation";

$$I_{AC}(\tau) \propto \int_{-\infty}^{\infty} I(t)I(t-\tau)\,dt \tag{4.2}$$

"$I(t)$ being the intensity of the input pulse. Since the phase of the pulse is not conserved, Equation (4.2) does not contain full information about the pulse. However, if the pulse shape is known, the pulse width can be calculated by deconvolution of the correlation."

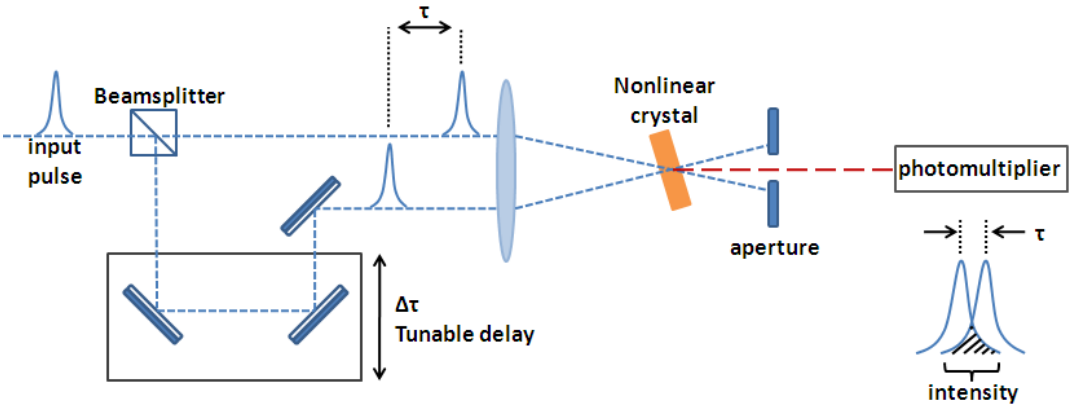

Figure 4.4 The diagram of an intensity autocorrelation.

Assuming a Gaussian pulse shape, a deconvolution factor of 0.707 is used in Equation (4.3) [46] , leading to pulse width. The result is shown in Fig. 4.5.

$$\Delta\tau_{Pulse}^{FWHM} = 0.707\Delta\tau_{Autocorrelation}^{FWHM} \tag{4.3}$$

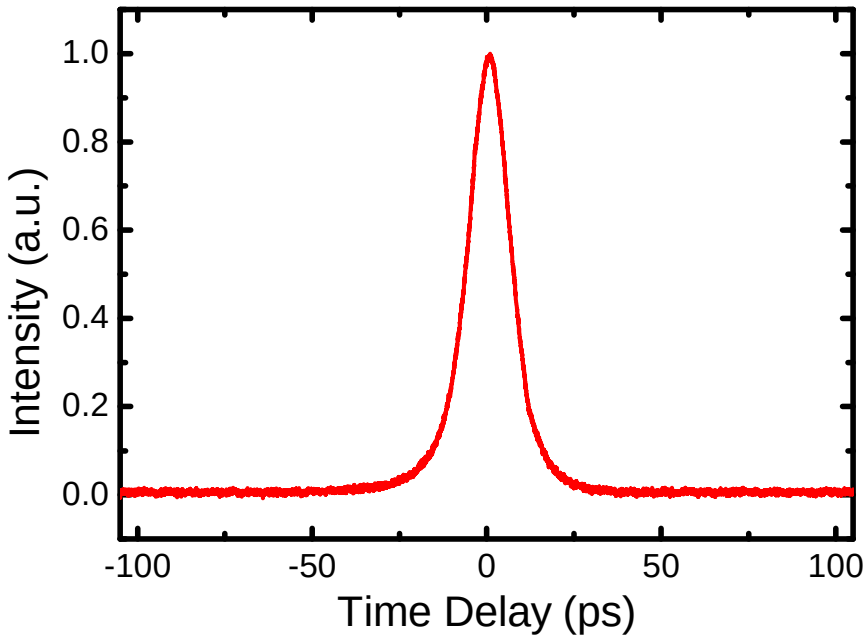

Figure 4.5 Autocorrelation result of the oscillator output from 30% port of coupler.

The measurement result of the oscillator pulses is shown in figure 4.5. The autocorrelation result at FWHM width is 14 ps. The pulse shape is assumed to be a Gaussian so that the corresponding pulse duration is estimated approximately as 10 ps. The long-range up to 200 ps autocorrelation result indicates no secondary pulses. In addition, no periodic modulation on the optical spectrum supports this result which was measured by 0.015nm wavelength resolution which is shown in figure 4.5.

4.3.2 Optical Spectrum and Pulse Train Measurements of Oscillator

If too much energy is accumulated inside the cavity, the laser will go into multiple-pulsing. To ensure proper operation of the laser, multiple-pulsing should be avoided. Optical spectrum together with the pulse train on the oscilloscope is used to check the presence of multiple-pulsing. Fig.4.6 and 4.7 show clear traces of these two measurements.

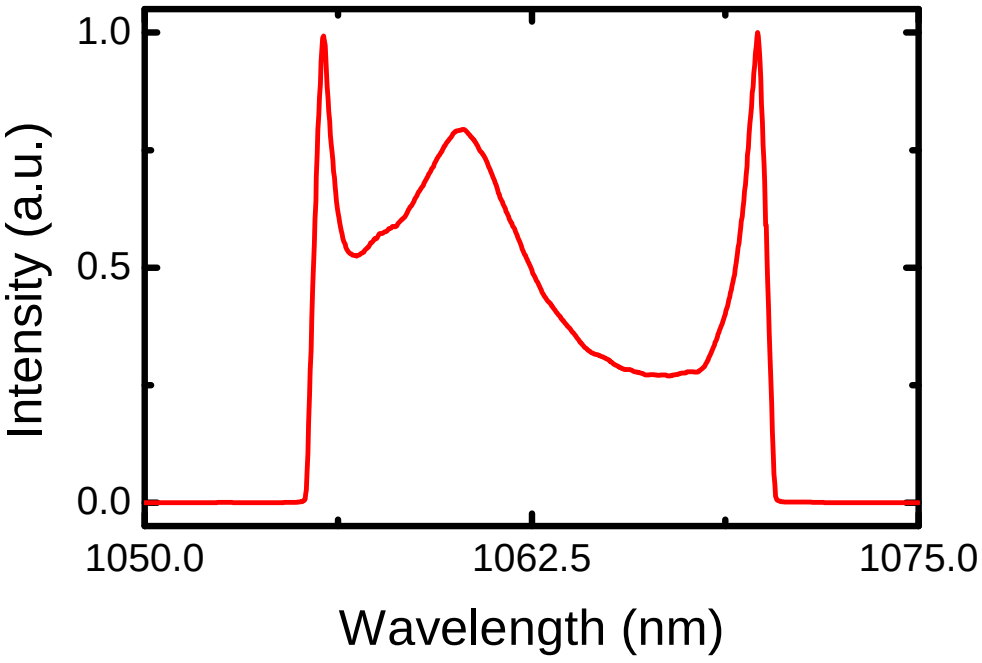

Figure 4.6 Measured spectra obtained from oscillator output

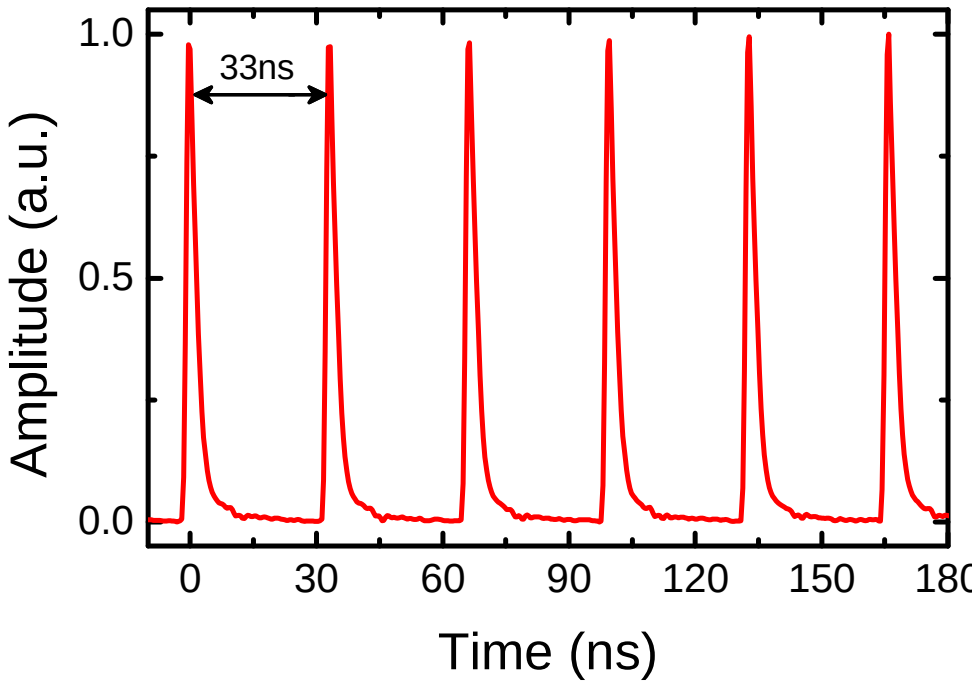

Figure 4.7 Pulse train of oscillator output

4.3.3 Summary for oscillator characterization

Table 4.2 Summary of oscillator parameters

Repetition rate	30 MHz
Average power (from 30% port of coupler)	65mW
Pulse energy	2.16nJ
Pulse width at FWHM	10 ps
Peak power	220 W
Spectral bandwidth at FWHM	14.6nm
Central wavelength	1062nm

4.4 Amplifier System

The amplifier system of the laser consists of two main parts which are the preamplifier and power amplifier. The diagram of the amplifier system is shown in Fig 4.8. The oscillator output power of 65 mW at 30 MHz is acquired directly from 30% port of output coupler after the Yb-doped fiber. The output fiber of oscillator is spliced to input of the amplifier system so that the coupling efficiency is improved and alignment error is completely eliminated for this point.

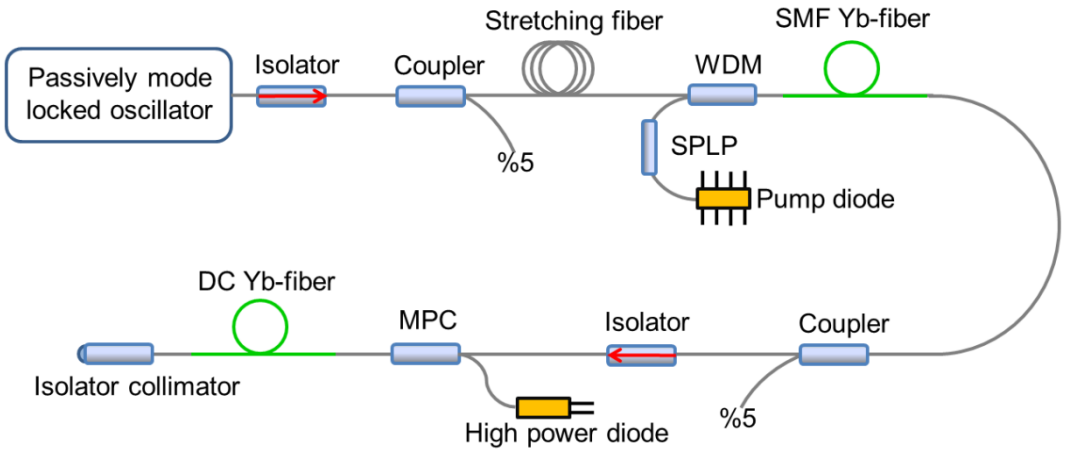

Figure 4.8 Amplifier system diagram for the laser.

The amplifier system begins with an isolator to protect the oscillator from back reflected signals. Also, it is necessary that the output power of the seed laser is enough for preamplifier stage in order to suppress the amplified spontaneous emission (ASE) which is due to the gain peak of Yb at 1030 nm. After the isolator, about %95 of the output power from the seed laser passes through a 100m long SMF stage to stretch the pulses. The remaining signal is reserved for monitoring purposes. Preamplifier is placed in order to ensure the reliable signal power for the power amplifier. The signal level of approximately 100mW or more can be sufficient for both suppressing of ASE and

saturation of power amplifier. This assumption comes from purely the experimental observation of our past project which is the nanosecond fiber laser source and its high power amplifier. The preamplifier stage comprises of a 0.5 m Yb-doped fiber which is same as in the oscillator pumped in-core by a 976 nm laser diode over WDM. In addition to that, single-mode pump protection SPLP is added after the pump diode to protect the diode from back reflected light. After the preamplifier, a 5/95 coupler and isolator is placed for monitoring and protection purposes, respectively.

In the power amplifier stage forward pumping structure is preferred in order to protect the pump diodes from the damage from a returning peak power signal to the pump ports. Pump coupling to the gain fiber is achieved by multi-port-combiner (MPC) whose pump port fiber is a multimode fiber (core diameter of 105 μm, 0.46NA). The signal port of the MPC is a large mode area (LMA) fiber (core diameter of 20 μm, 0.07NA). After second isolator, 250 mW of signal power is coupled to the output fiber of the MPC. There one 975 nm diodes whose maximum output power is 25 W was used. The diode which was coupled to 105 μm core diameter multimode fibers is used as a pump for the power amplifier. The empty pump port is used for monitoring the power. The high-power amplifier housed a 2.5 m long LMA double clad (DC) Yb-doped fiber that has similar attributes as with the MPC signal fiber. The DC fiber which is the gain medium for amplifiers has 9×10^{25} m^{-3} of ytterbium doping concentration. The MPC output fiber is spliced to the gain fiber. The stripping region on the outer cladding is recoated using a low-index polymer to avoid pump loss through the splice region. Finally, gain fiber is spliced to the fiber of the isolator-collimator. The task of the isolator is to not allow the reflected beam coupling back into the laser system. In addition, the gain fiber was coiled to about 10 cm diameter to improve the output beam quality of power amplifier. The main idea for suitable small coiling is to prevent the excitation of higher order transverse electromagnetic modes (TEM). Photo of the mode locked Yb-doped fiber laser amplifier is shown in figures 4.9-11.

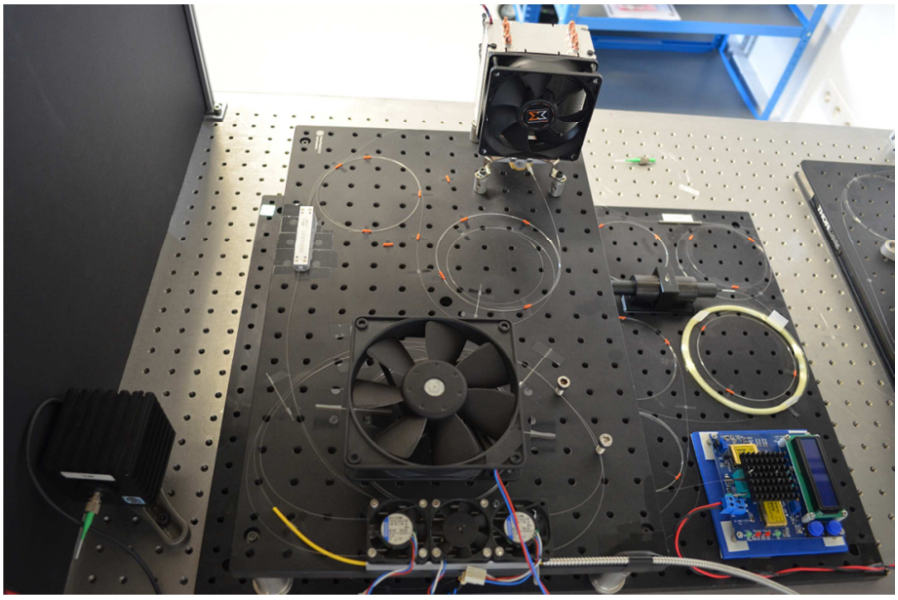

Figure 4.9 The implemented amplifier system for the laser. The ground floor contains preamplifier and the upper floor contains power amplifier.

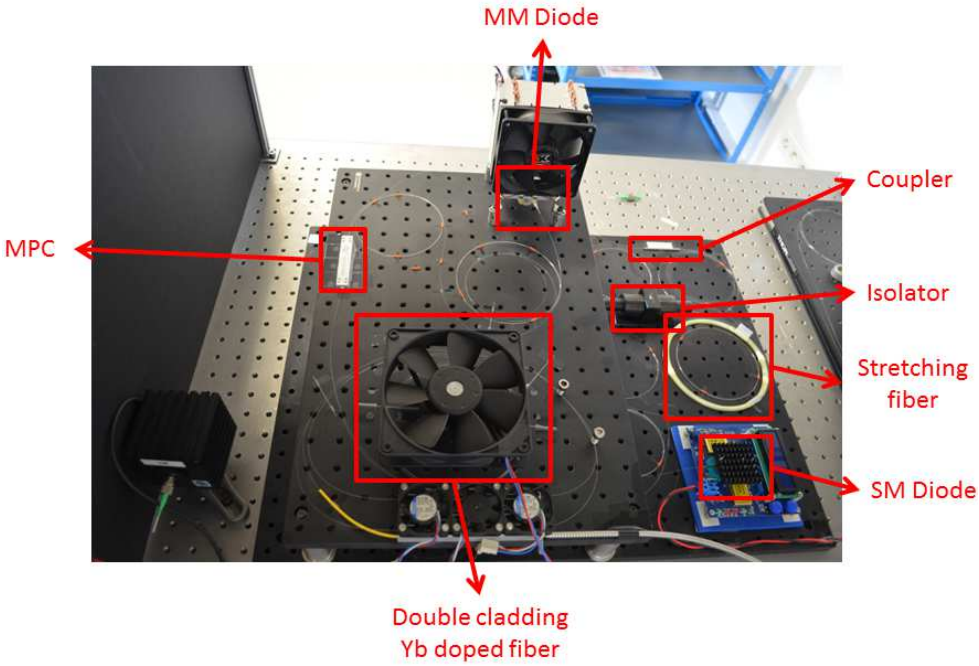

Figure 4.10 The labeled photo of the implemented amplifier system for the laser.

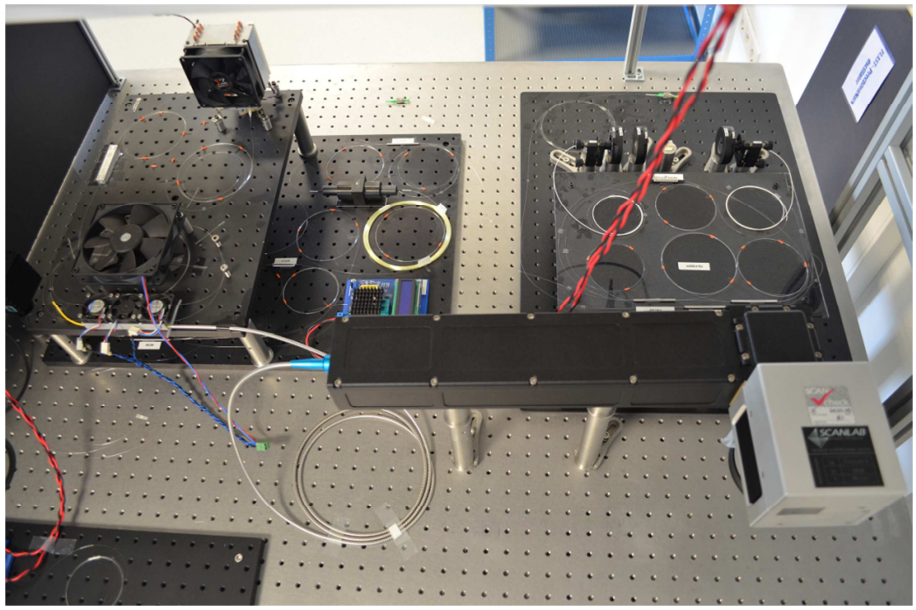

Figure 4.11 The all fiber laser system.

4.5 Amplifier Characterization

4.5.1 Autocorrelation Measurement of Amplifier System

The autocorrelation measurement result of the pulses at 15 W (red line in graph) of average power is shown in Fig. 4.12. The autocorrelation result of 15 W at FWHM width is 71 ps. The pulse shape is assumed to be a Gaussian so that the corresponding pulse duration is estimated approximately as 50 ps. The long-range up to 200 ps autocorrelation result indicates no secondary pulses. In addition, no periodic modulation on the optical spectrum supports this result which was measured by 0.015nm wavelength resolution which is shown in figure 4.5.

Besides, variation of FWHM pulse width was observed with different average power levels. The pulse width as a function of the output power is shown in Fig. 4.13. The pulse width decreases with power because of successive gain narrowing. When gain narrowing happens in power amplifier, the highly chirped pulse losses some longer wavelength components so that the pulse width become shorter.

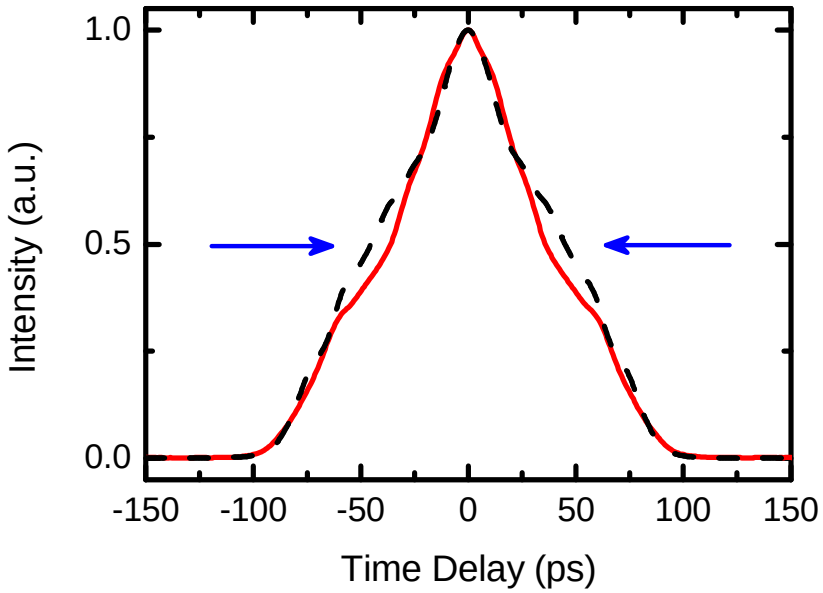

Figure 4.12 The autocorrelation measurement results. The solid red line measured at 15 W and the dashed line at 1 W

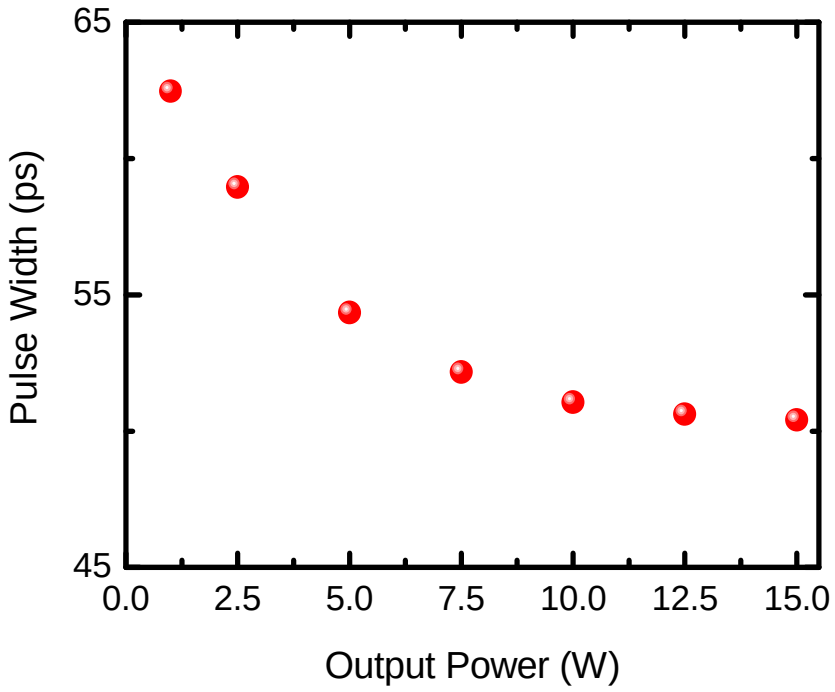

Figure 4.13 The pulse width as a function of the output power

4.5.2 Optical Spectrum and Power Scaling Measurement

The optical spectrum of the preamplifier and power amplifier measured after the stretching stage. As shown figure 4.8, pulses of the oscillator are temporally stretched in a 100 m long SMF stage. The broadened pulses pass through the preamplifier stage which includes 0.5 m long SMF Yb-fiber. The result of the spectral measurement of the pulse after the preamplifier is displayed in Fig. 4.14. The spectral width is expanded slightly to 16.6 nm and some oscillations are observed at the edges of the spectrum because of nonlinearity. There is no major ASE signal at the gain peak of 1030 nm, nor a stimulated Raman scattering (SRS) signal at longer wavelengths. The optical spectrum at 15 W measured after power amplifier is shown Fig. 4.15. At 15 W of average power, the pulse energy is about 500 µJ and the peak power is estimated at 10 kW. Some oscillations develop on the spectrum at high powers due to nonlinear effects. It is hard to say which nonlinear effects create oscillation on spectrum however the possible strongest nonlinear effect is self-phase modulation

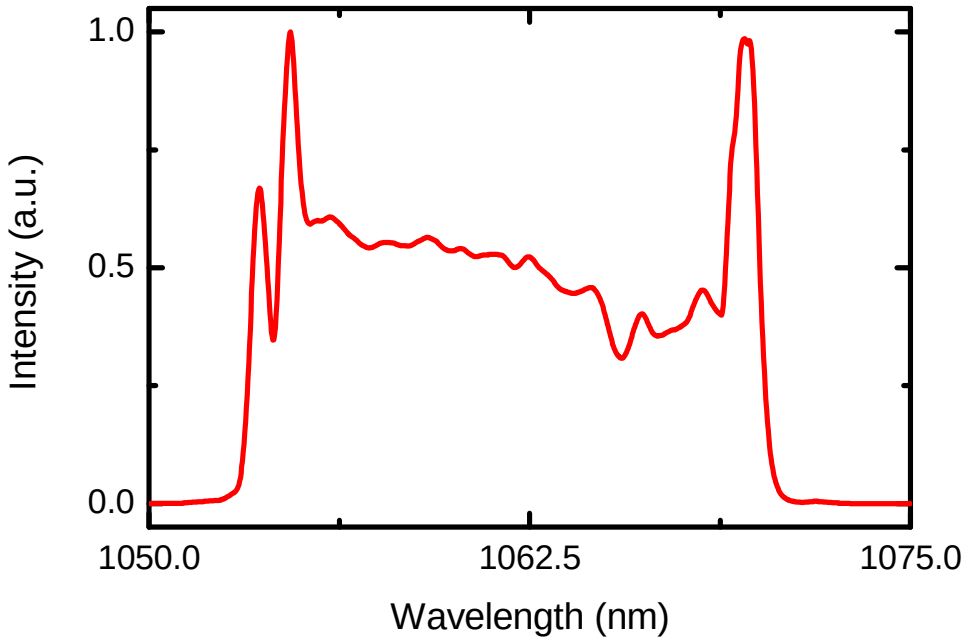

Figure 4.14 Measured spectra obtained from preamplifier output.

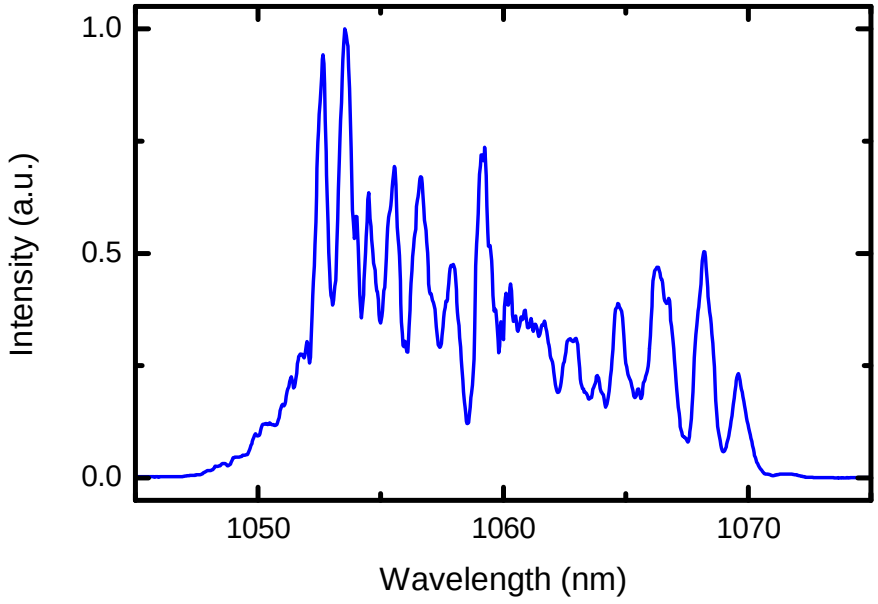

Figure 4.15 Measured spectra obtained from the power amplifier output at 15 W.

Experimentally measured signal power as a function of pump power is shown in Fig. 4.16. Output signal power was measured at 15 W from the isolator-collimator output of a total coupled pump power of 22 W. Optical conversion efficiency is calculated to be about 70%. The deviation of the measured values from lower pump powers to high pump power is due to shift of the diode emission wavelength. At low pump powers, the peak emission wavelength from the diodes is around 960–965 nm, which is far away from the peak absorption wavelength (~976 nm) of a Yb-doped fiber. This deviation can be compensated by increasing the diode temperature. As the diode drive current is increased, the emission wavelength shifts toward 976 nm.

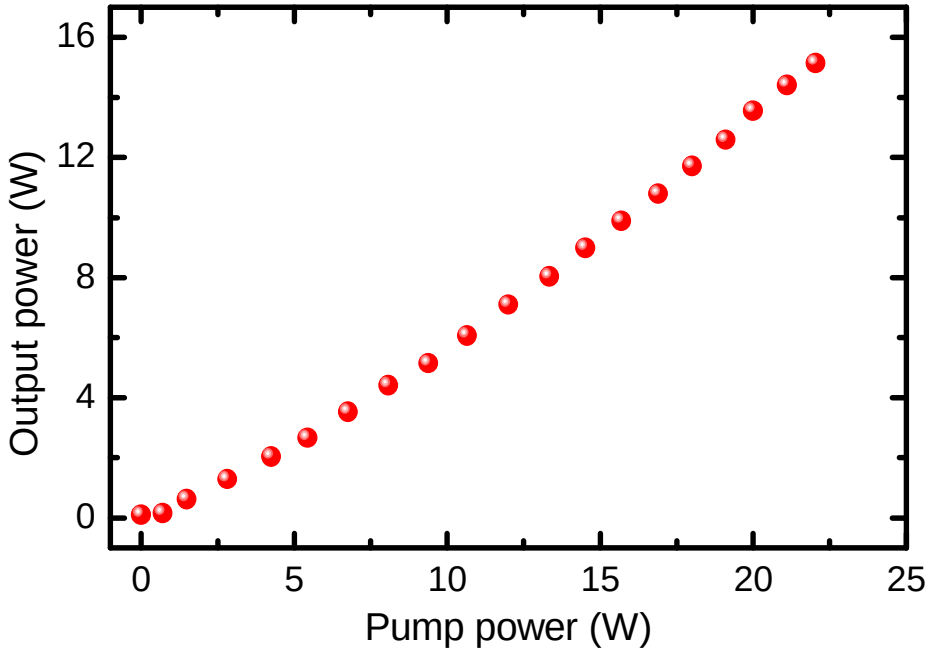

Figure 4.16 Measured signal power as a function of pump power.

4.5.3 Summary for Power Amplifier Characterization

Table 4.3 Summary of power amplifier parameters

Repetition rate	30 MHz
Average power	15W
Pulse energy	500nJ
Pulse width at FWHM (15W)	50 ps
Peak power	10kW
Central wavelength	1062nm

CHAPTER 5

CONCLUSION

Fiber lasers are commonly used in many areas including materials processing, medical, metrology, and defense applications. Fiber lasers have some special advantages against common solid-state lasers. Their excellent beam quality, power scalability, high efficiency and alignment-free operation are some of those advantages. Thus, the application areas of fiber lasers are continuously increasing proportional to their maximum output power level, which is increasing at a rate of approximately 1.7-times per year for the past decade. For many applications, flexibility and misalignment-free operation is important. In this thesis, we constructed a picosecond pulsed ytterbium doped fiber laser source and amplifier.

After introducing the fiber lasers in chapter one, we summarized the basic theoretical background of nonlinear optics and fiber laser in chapter two. The chapter covered parametric and nonparametric processes for nonlinear optics and included pulse propagation, mode locking theory, amplification process and main limitations for fiber lasers.

The developed fiber laser system was based on a master oscillator power amplifier (MOPA) configuration. The system consisted of two main parts which were seed laser and amplifiers. The seed laser was a passively mode-locked ytterbium (Yb) doped fiber laser oscillator, i.e. ring fiber laser which had an isolator to ensure unidirectional round trips. In passive mode locking, the method of nonlinear polarization evolution (NPE) was used as a saturable absorber in the oscillator. The implemented fiber laser oscillator showed stable 10 picoseconds (ps) pulses with a 30 MHz repetition rate. The central wavelength of the oscillator was at 1062 nm because of the transmission bandwidth of the isolator. The spectral bandwidth of the oscillator was about 14 nm with obtaining 65 mW average output power at output port which was used in amplifier stages. The corresponding pulse energy and peak power for output port was about 2.2 nJ and 220 W, respectively. The all characteristics and discussion of the oscillator about experimental work were reported in the chapter four.

After the development of the laser oscillator, the preamplifier and power amplifier stages were constructed. The preamplifier mainly consisted of two parts which were pulse stretcher and core-pumped amplifier. In order to store more energy in per pulse a pulse stretcher was used before the amplifiers. The pulse stretcher was 100 m single mode fiber which had positive dispersion around 1060 nm so that the oscillator pulse duration 10 ps increased 62 ps after the stretcher. Then the laser signal amplified to 265 mW by a single mode Yb-doped fiber. The optical pumping scheme of the preamplifier was forward core pumped and the wavelength of the pump diode was 976 nm. After this stage, the laser signal amplified by a forward cladding-pumped power amplifier with double clad Yb-doped large mode area fiber. The amplifier was pumped by 22 W at 976 nm and the output power was measured at 15 W, the corresponding optical conversion efficiency is estimated %70. The spectral measurement after amplifiers showed that the some oscillations develop on the spectrum at high powers due to nonlinear effects. Besides, Amplified spontaneous emission and stimulated Raman scattering was not observed. At 15 W of average power, the pulse duration and pulse energy were about 50 ps and 500nJ, respectively. The corresponding peak power was estimated approximately 10 kW. The all characteristics and discussions of the amplifiers about experimental work were

reported in the chapter four. During the all design and optimization process, the numerical simulation was used for the fiber laser system. The simulation was based on nonlinear Schrödinger equation with the method of split-step evaluation. The brief theoretical background and simulation results of the laser system were reported in chapter three.

The developed fiber laser system can be used in material processing with high precision, spectroscopy, and medicine.

REFERENCES

[1] J. L. Baird, British Patent 285,738 (1928).

[2] C. W. Hansell, U. S. Patent 1,751,584 (1930).

[3] H. Lamm, “Biegsame optische gerate,” Z. Instrumenten. 50, 579 (1930).

[4] A. C. S. van Heel, “A new method of transporting optical images without aberrations,” Nature 173, 39 (1954).

[5] H. H. Hopkins and N. S. Kapany, “A flexible fiberscope using static scanning,” Nature 173, 39 (1954).

[6] B. O’Brian, U. S. Patent 2,825,260 (1958).

[7] B. I. Hirschowitz, U. S. Patent 3,010,357 (1961).

[8] T. Miya, Y. Terunuma, T. Hosaka, and T. Miyashita, “Ultimate low-loss single-mode fibre at 1.55 μm,” Electron. Lett. 15, 106 (1979).

[9] http://www.fiberoptics4sale.com/wordpress/optical-fiber-attenuation, last visited on June 2012

[10] R. H. Stolen, E. P. Ippen, and A. R. Tynes, “Raman oscillation in glass optical waveguide,” Appl. Phys. Lett. 20, 62 (1972).

[11] E. P. Ippen and R. H. Stolen, “Stimulated Brillouin scattering in optical fibers,” Appl. Phys. Lett. 21, 539 (1972).

[12] R. G. Smith, “Optical power handling capacity of low loss optical fibers as determined by stimulated Raman and Brillouin scattering,” Appl. Opt. 11, 2489 (1972).

[13] R. H. Stolen and A. Ashkin, “Optical Kerr effect in glass waveguide,” Appl. Phys. Lett. 22, 294 (1973).

[14] R. H. Stolen, J. E. Bjorkholm, and A. Ashkin, “Phase-matched three-wave mixing in silica fiber optical waveguides,” Appl. Phys. Lett. 24, 308 (1974). 131

[15] K. O. Hill, D. C. Johnson, B. S. Kawasaki, and R. I. MacDonald, “CW three-wave mixing in single-mode fibers,” J. Appl. Phys. 49, 5098 (1974).

[16] R. H. Stolen, “Phase-matched-stimulated four-photon mixing in silica-fiber waveguides,” IEEE J. Quantum Electron. QE-11, 100 (1975).

[17] R. H. Stolen and C. Lin, “Self-phase-modulation in silica optical fibers,” Phys. Rev. A 17, 1448 (1978).

[18] A. Hasegawa and F. Tappert, “Transmission of stationary nonlinear optical pulses in dispersive dielectric fibers. I. Anomalous dispersion,” Appl. Phys. Lett. 23, 142 (1973).

[19] L. F. Mollenauer, R. H. Stolen, and J. P. Gordon, “Experimental observation of picosecond pulse narrowing and solitons in optical fibers,” Phys. Rev. Lett. 45, 1095 (1980).

[20] I. N. Duling III, “Subpicosecond all-fibre erbium laser,” Electron. Lett. 27, 544-545 (1991).

[21] K. Tamura, C. R. Doerr, H. A. Haus, and E. P. Ippen, “Soliton fiber ring laser stabilization and tuning with a broad intracavity filter,” IEEE Phot. Tech. Lett. 6, 697-699 (1994).

[22] K. Tamura, E. P. Ippen, H. A. Haus, and L. E. Nelson, “77-fs pulse generation from a stretched-pulse mode-locked all-fiber ring laser,” Opt. Lett. 18, 1080-1082 (1993).

[23] F. Ö. Ilday, J. R. Buckley, W. G. Clark, and F. W. Wise, “Self-similar evolution of parabolic pulses in a laser,” Phys. Rev. Lett. 92, 3902-3905 (2004).

[24] J. R. Buckley, F. Ö. Ilday, F. W. Wise, “Femtosecond fiber lasers with pulse energies above 10 nJ,” Opt. Lett. 30, 1888-1890 (2005).

[25] A Chong, J Buckley, W Renninger, F Wise, “All-normal-dispersion femtosecond fiber laser,” Opt. Exp. 14, 10095-10100 (2006).

[26] B. Oktem, C. Ülgüdür and F. Ö. Ilday, "Soliton-similariton fibre laser", Nature Photonics, 4, 307, (2010). 132

[27] E. Snitzer, H. Po, F. Hakimi, R. Tumminelli, B. C. McCollum, “Double clad offset core Nd fiber laser”, Optical Fiber Sensors Topical Meeting, New Orleans, Louisiana/USA, paper PD 5, (1988).

[28] http://www.ipgphotonics.com/, last visited on June 2012

[29] R. W. Boyd, *Nonlinear Optics* (Academic Press, 2003).

[30] G. P. Agrawal, *Nonlinear Fiber Optics* (Academic Press, 2007).

[31] G. P. Agrawal, *Applications of Nonlinear Fiber Optics* (Academic Press, 2001).

[32] P. W. Milonni and J. H. Eberly, *Lasers* (Wiley Interscience, 1988).

[33] G.P. Agrawal, “Optical Pulse Propagation in Doped Fiber Amplifiers,” Phys.Rev.A **44**, 7493-7501 (1991).

[34] RP Photonics, ytterbium doped gain media http://www.rp-photonics.com/ ,last visited on June 2012

[35] H. A. Haus, E. P. Ippen, and J. G. Fujimoto, “Structures for Additive Pulse Mode Locking,” J. Opt. Soc. Am. B **8**, 2068-2078 (1991).

[36] Kaertner, F. X., *Mode locked laser theory*, 2006.

[37] New, G.H.C., *Pulse evolution in mode-locked quasicontinuous lasers*, IEEE J.Quantum Electron. 10, 115-124, 1974.

[38] Haus, H. A., *Mode locking of lasers*, IEEE J. Selec. Top. Quan. Electron. 6,1173, 2000.

[39] Haus, H. A., *A Theory of Forced Mode Locking*, IEEE Journal of Quantum Electronics QE-11, pp. 323 – 330, 1975.

[40] M. Hofer, M. E. Fermann, F. Haberl, M. H. Ober, and A. J. Schmidt, "Mode Locking with Cross-Phase and Self-Phase Modulation," Opt. Lett. **16**, 502-504 (1991).

[41] RP Photonics, www.rp-photonics.com/passive_mode_locking.html, last visited on June 2012

[42] J. S. Russell, "Report of the fourteenth meeting of the British Association for the Advancement of Science", York, September 1844 (London 1845), pp 311-390, Plates XLVII-LVII.

[43] E.P. Ippen, C.V. Shank, "Ultrashort Light Pulses", S.L. Shapiro ed., New York: Springer-Verlag (1977)

[44] M. Erdogan,B. Oktem, H.Kalaycıoglu, S.Yavas, P. K. Mukhopadhyay, K. Eken, K. Ozgoren, Y. Aykac, U. H. Tazebay, and F. O. Ilday, "Texturing of titanium (Ti6Al4V) medical implant surfaces with MHz-repetition-rate femtosecond and picosecond Yb-doped fiber lasers" Opt. Exp. 19, 10986 (2011).

[45] B. Oktem, H. Kalaycioglu, M. Erdoğan, S. Yavaş, P. Mukhopadhyay, U. H. Tazebay, Y. Aykaç, K. Eken, and F. Ö. Ilday, "Surface texturing of dental implant surfaces with an ultrafast fiber laser," in Conference on Lasers and Electro-Optics, OSA Technical Digest (CD) (Optical Society of America, 2010), paper JTuD15.

[46] K. Ozgoren, B. Oktem, S.Yılmaz, K. Eken, and F. O. Ilday, "83W, 3.1 MHz, square-shaped, 1 ns-pulsed all-fiber-integrated laser for micromachining" Opt. Exp. 19, 17647 (2011).